Efficient well–balanced hydrostatic upwind schemes for shallow–water equations

Christophe Berthon [a] Françoise Foucher [a,b]

[a] *Laboratoire de Mathématiques Jean Leray, CNRS UMR 6629, Université de Nantes, 2 rue de la Houssinière, BP 92208, 44322 Nantes cedex 3, France.*

[b] *Ecole Centrale de Nantes, 1 rue de La Noë, BP 92101 44 321 Nantes cedex 3, France*

Abstract

The proposed work concerns the numerical approximations of the shallow-water equations with varying topography. The main objective is to introduce an easy and systematic technique to enforce the well-balance property and to make the scheme able to deal with dry areas. To access such an issue, the derived numerical method is obtained by involving the free surface instead of the water height and this produces the scheme well-balanced independently from the numerical flux function associated with the homogeneous problem. As a consequence, we obtain an easy well-balanced scheme which preserves non negative water height. When compared with the well-known hydrostatic reconstruction, the presented topography discretization does not involve any max function known to introduce some numerical errors as soon as the topography admits very strong variations or discontinuities. A second-order MUSCL accurate reconstruction is adopted. The proposed hydrostatic upwind scheme is next extended for considering 2D simulations performed over unstructured meshes. Several 1D and 2D numerical experiments are performed to exhibit the relevance of the scheme.

Key words: shallow–water equations, finite volume schemes, source term approximations, well–balanced schemes, positive preserving schemes

1 Introduction

In the present work, we consider the derivation of numerical methods to approximate the solutions of the shallow-water equations. When assuming a smooth topography $z : \mathbb{R}^2 \to \mathbb{R}^+$, the Saint-Venant model describes the evolution of both water height, denoted h, and velocity vector (u, v) in the plane parallel to the bottom. The model under consideration is governed by the following set of partial differential equations:

$$\begin{cases} \partial_t h + \partial_x hu + \partial_y hv = 0, \\ \partial_t hu + \partial_x (hu^2 + \frac{g}{2}h^2) + \partial_y huv = -hg\partial_x z, \\ \partial_t hv + \partial_x huv + \partial_y (hv^2 + \frac{g}{2}h^2) = -hg\partial_y z, \end{cases} \tag{1.1}$$

where $g > 0$ stands for the gravity constant.

From now on, let emphasize that the definition of the topography function is free from the location of the bottom. In general, the bottom is fixed so that $\min z(x) = 0$, but other reference bottom can bee chosen (for instance, see [3,44,46,13]). In fact, in the forthcoming derivation, the location of the bottom will be crucial and we adopt the following convention:

$$\min z(x) = z_0. \tag{1.2}$$

The model (1.1) is known to be hyperbolic over the space of admissible states Ω_2 defined as follows:

$$\Omega_2 = \left\{ {}^t(h, hu, hv) \in \mathbb{R}^3;\ h > 0 \right\}.$$

Moreover, this model preserves the steady state of a lake at rest defined by

$$h + z = \text{cst} \quad \text{and} \quad u = 0.$$

In order to ensure the relevance of a numerical method approximating the solutions of (1.1), the scheme must preserve non-negative water height but also it must be well-balanced [3], *i.e.* it exactly captures the lake at rest solutions.

After the work proposed by Greenberg et al. [29,30] and next by Gosse [26], numerous schemes have been derived according to the well-balance strategy [8,10,11,19–21,23,32–34,45,53]. The main difficulty comes from the derivation of a suitable discretization of the topography source term in order to be consistent with the lake at rest. More recently, Audusse et al. [1] introduced a procedure which makes the source term discretization well-balanced independently from the discretization of the transport operator, the well-known hydrostatic reconstruction. This technique is based on a water height reconstruction procedure to define on each side of a cell interface:

$$h^-_{i+\frac{1}{2}} = \max(0, h^n_i + z_i - z_{i+\frac{1}{2}}) \quad \text{and} \quad h^+_{i+\frac{1}{2}} = \max(0, h^n_{i+1} + z_{i+1} - z_{i+\frac{1}{2}}),$$

where we have set $z_{i+\frac{1}{2}} = \max(z_i, z_{i+1})$.

This reconstruction is next considered to obtain schemes which are both non-negative water height preserving and well-balanced. In fact, one of the main interest of the hydrostatic reconstruction approach stays in its genericity. Indeed, it can be applied with any given numerical flux function for homogeneous Saint-Venant equations (with constant topography). This crucial property makes the hydrostatic reconstruction very attractive and it is now widely used (for instance, see [2,43,7,44]).

However, in a recent study, Delestre [18] exhibited some numerical failures when considering large topography variations on a coarse mesh. Indeed, as soon as $z_{i+\frac{1}{2}} - z_i > h_i^n$, the hydrostatic reconstruction enforce $h^-_{i+\frac{1}{2}} = 0$ and some wrong solutions thus may occur. Nevertheless, for a smooth topography, we have $z_{i+\frac{1}{2}} - z_i = O(\Delta x)$, where Δx denotes the mesh size, and such a failure no longer stays for Δx small enough. However, when considering simulations of physical interest, it is very difficult to predict a relevant size mesh in order to avoid wrong behavior of the hydrostatic reconstruction.

The main purpose of the present paper is to propose an alternative to the hydrostatic reconstruction which does not involve wrong approximations as soon as the topography admits strong variations. Similarly to the hydrostatic reconstruction, the obtained scheme must satisfy the following properties:

(i) an easy discretization of the topography source term free from the choice of the numerical flux function associated with the approximation of the homogeneous shallow-water equations,
(ii) the preservation of non-negative water height,
(iii) the preservation of the lake at rest (the well-balance property).

The paper is organized as follows. In the next section, we present the adopted strategy in the case of the 1D model. According to Kurganov's work [9], the main idea consists by introducing the free surface into the model to obtain a suitable reformulation. As a consequence, the standard shallow-water flux function involves the free surface instead of the water depth. Based on this argument, we derive a numerical procedure to modify any finite volume scheme given for the homogeneous shallow-water equations in order to deal with non-flat topography. In addition, the resulting very flexible scheme turns out to be computationally non-expensive. In section 3, we show the relevance of the method by establishing the main properties satisfied by the approximate solutions. Indeed, the scheme is proved to be well-balanced and to preserve the water height non-negative. The following section is devoted to second-order extension by considering a standard MUSCL technique [38,41,51]. The obtained accurate numerical scheme is, once again, proved to be well-balanced and non-negative water height preserving. Next, in section 5, we give the 2D scheme over an unstructured mesh and we show that all the requirements (i)-(ii)-(iii) are satisfied. This makes the method very efficient since it is robust (satisfying properties (ii) and (iii)) but also very easy to be implemented (property (i)). In fact, starting from a basic scheme which approximates the homogeneous shallow-water equations on unstructured meshes, we will see that the modification to take into account a varying topography will turn out to be obvious. Section 6 is devoted to illustrate the interest of the scheme by performing numerous numerical experiments. A conclusion completes the paper.

2 Derivation of hydrostatic upwind schemes

For the sake of clarity in the presentation of our numerical strategy, first, we focus on the 1D model given as follows:

$$\begin{cases} \partial_t h + \partial_x hu = 0, \\ \partial_t hu + \partial_x (hu^2 + \frac{g}{2}h^2) = -hg\partial_x z. \end{cases} \tag{2.1}$$

The space of admissible states is here given by

$$\Omega_1 = \left\{ {}^t(h, hu) \in \mathbb{R}^2;\ h > 0 \right\}.$$

To shorten the notations, let us rewrite this model into the following form:

$$\partial_t w + \partial_x f(w) = S(w), \tag{2.2}$$

with

$$w = \begin{pmatrix} h \\ hu \end{pmatrix}, \quad f(w) = \begin{pmatrix} hu \\ hu^2 + \frac{g}{2}h^2 \end{pmatrix} \quad \text{and} \quad S(w) = \begin{pmatrix} 0 \\ -gh\partial_x z \end{pmatrix}, \tag{2.3}$$

where $w : \mathbb{R} \times \mathbb{R}^+ \to \Omega_1$ is the unknown state vector, $f : \Omega_1 \to \mathbb{R}^2$ stands for the flux function and $S : \Omega_1 \to \mathbb{R}^2$ is the topography source term.

The suggested numerical strategy lies on a suitable reformulation of the system (2.1). We introduce the free surface H and the fraction of water X defined as follows:

$$H = h + z \quad \text{and} \quad X = \frac{h}{H}. \tag{2.4}$$

As underlined in the introduction, the model under consideration is free from the location of the bottom. According to the convention (1.2), we fix the constant z_0 such that $H(x,t) > 0$ over the whole domain of computation. Now, let us remark the identity:

$$h^2 = XH^2 - hz,$$

to write (2.1) in the following form:

$$\begin{cases} \partial_t h + \partial_x X H u = 0, \\ \partial_t hu + \partial_x \left(X \left(Hu^2 + \frac{g}{2} H^2 \right) - \frac{g}{2} hz \right) + gh\partial_x z = 0. \end{cases} \tag{2.5}$$

Next, we introduce a state vector

$$W = \begin{pmatrix} H \\ Hu \end{pmatrix}, \tag{2.6}$$

which is nothing but the state vector w associated with the free surface. Arguing these notations, the system (2.5) now reads:

$$\partial_t w + \partial_x \left(X f(W) - \begin{pmatrix} 0 \\ \frac{g}{2} hz \end{pmatrix} \right) + \begin{pmatrix} 0 \\ gh\partial_x z \end{pmatrix} = 0. \tag{2.7}$$

Let us emphasize that both formulations (2.2) and (2.7) are rigorously equivalent and we decide to consider (2.7) to derive numerical schemes. We consider a uniform mesh of size $\Delta x = x_{i+\frac{1}{2}} - x_{i-\frac{1}{2}}$ and we denote by Δt the time step so that we define $t^{n+1} = t^n + \Delta t$. At time t^n we assume known a piecewise constant approximation of the solution w. On the cell $(x_{i-\frac{1}{2}}, x_{i+\frac{1}{2}})$ we denote $w_i^n = {}^t(h_i^n, h_i^n u_i^n)$ the constant approximation. We set

$$H_i^n = h_i^n + z_i \quad \text{and} \quad X_i^n = \frac{h_i^n}{H_i^n}. \tag{2.8}$$

We now evolve this approximation at time t^{n+1}. To address such an issue, we enforce the acknowledgement of a finite volume scheme to approximate the weak solutions of the homogeneous Saint-Venant model (*i.e.* $z = \text{cst}$) as follows:

$$(w^{\text{homo}})_i^{n+1} = w_i^n - \frac{\Delta t}{\Delta x} \left(f_{\Delta x}(w_i^n, w_{i+1}^n) - f_{\Delta x}(w_{i-1}^n, w_i^n) \right), \tag{2.9}$$

where $f_{\Delta x} = {}^t(f_{\Delta x}^h, f_{\Delta x}^{hu}) : \Omega_1 \times \Omega_1 \to \mathbb{R}^2$ stands for the numerical flux function given by any approximation technique (for instance HLL and HLLC schemes [31,51], relaxation schemes [8,16,17,42,35], VFRoe scheme [21,23,22]). Of course, the function $f_{\Delta x}$ is assumed to be consistent with the exact flux function and it thus satisfies:

$$f_{\Delta x}(w, w) = f(w) \quad \text{for all } w \in \Omega_1. \tag{2.10}$$

As usual, in order to rule out some instabilities, the homogeneous scheme (2.9) is endowed with a CFL like condition given by:

$$\frac{\Delta t}{\Delta x}\max_{i\in\mathbb{Z}}|\lambda^{\pm}(w_i^n,w_{i+1}^n)|\leq\frac{1}{2},\tag{2.11}$$

where $\lambda^{\pm}(w_i^n,w_{i+1}^n)$ denotes some numerical larger and smaller eigenvalues associated to the definition of the numerical flux function $f_{\Delta x}$. In addition, we here impose the homogeneous scheme (2.9) to be Ω_1-preserving; *i.e.* as long as $w_i^n\in\Omega_1$ for all $i\in\mathbb{Z}$, we have $(w^{\text{homo}})_i^{n+1}\in\Omega_1$.

Now, to derive a numerical approximation of (2.5), we modify the homogeneous scheme (2.9) to introduce the topography source term. The adopted scheme is given by:

$$\begin{cases} h_i^{n+1}=h_i^n-\frac{\Delta t}{\Delta x}(X_{i+\frac12}f^h_{\Delta x}(W_i^n,W_{i+1}^n)-X_{i-\frac12}f^h_{\Delta x}(W_{i-1}^n,W_i^n)),\\ (hu)_i^{n+1}=(hu)_i^n-\dfrac{\Delta t}{\Delta x}\left(X_{i+\frac12}f^{hu}_{\Delta x}(W_i^n,W_{i+1}^n)-X_{i-\frac12}f^{hu}_{\Delta x}(W_{i-1}^n,W_i^n)\right)\\ \qquad\qquad +\dfrac{g}{2}\dfrac{\Delta t}{\Delta x}(h_{i+\frac12}z_{i+\frac12}-h_{i-\frac12}z_{i-\frac12})\\ \qquad\qquad -g\dfrac{\Delta t}{\Delta x}\dfrac{h_{i-\frac12}+h_{i+\frac12}}{2}(z_{i+\frac12}-z_{i-\frac12}), \end{cases}\tag{2.12}$$

where we have set for all i in $\mathbb{Z}$:

$$\begin{aligned} H_{i+\frac12}=&\bar H(W_i^n,W_{i+1}^n)\quad\text{with}\\ &\bar H(W_L,W_R)=\begin{cases}H_L & \text{if } f^h_{\Delta x}(W_L,W_R)>0,\\ H_R & \text{elsewhere,}\end{cases} \end{aligned}\tag{2.13}$$

$$\begin{aligned} X_{i+\frac12}=&\bar X(W_i^n,W_{i+1}^n,h_i^n,h_{i+1}^n)\quad\text{with}\\ &\bar X(W_L,W_R,h_L,h_R)=\begin{cases}X_L=\frac{h_L}{H_L} & \text{if } f^h_{\Delta x}(W_L,W_R)>0,\\ X_R=\frac{h_R}{H_R} & \text{elsewhere,}\end{cases} \end{aligned}\tag{2.14}$$

and

$$h_{i+\frac12}=H_{i+\frac12}X_{i+\frac12}\quad\text{and}\quad z_{i+\frac12}=H_{i+\frac12}(1-X_{i+\frac12}).\tag{2.15}$$

To conclude the presentation of the scheme, let us emphasize that it rewrites in a very convenient form. Indeed, from a straightforward computation we have:

$$\begin{aligned} (h_{i+\frac12}z_{i+\frac12}-h_{i-\frac12}z_{i-\frac12})-(h_{i-\frac12}+h_{i+\frac12})(z_{i+\frac12}-z_{i-\frac12})&=h_{i+\frac12}z_{i-\frac12}-h_{i-\frac12}z_{i+\frac12},\\ &=H_{i+\frac12}X_{i+\frac12}H_{i-\frac12}(1-X_{i-\frac12})-H_{i-\frac12}X_{i-\frac12}H_{i+\frac12}(1-X_{i+\frac12}),\\ &=H_{i-\frac12}H_{i+\frac12}(X_{i+\frac12}-X_{i-\frac12}), \end{aligned}$$

such that we obtain the following reformulation of (2.12):

$$
\begin{aligned}
w_i^{n+1} = w_i^n &- \frac{\Delta t}{\Delta x}(X_{i+\frac{1}{2}} f_{\Delta x}(W_i^n, W_{i+1}^n) - X_{i-\frac{1}{2}} f_{\Delta x}(W_{i-1}^n, W_i^n)) \\
&+ \frac{g}{2}\frac{\Delta t}{\Delta x}\begin{pmatrix} 0 \\ H_{i-\frac{1}{2}} H_{i+\frac{1}{2}} (X_{i+\frac{1}{2}} - X_{i-\frac{1}{2}}) \end{pmatrix}
\end{aligned}
\tag{2.16}
$$

Form now on, let us underline the role played by the location of the bottom. Indeed, as soon as the topography is flat, *i.e.* $z(x) = z_0$, the usual schemes (for instance, see [12,14,24,48,49]) no longer involve z since the discretization of the topography source term $gh\partial_x z$ vanishes. Here, the bottom location z_0 formally introduces some additional viscosity. For such a specific case, the scheme (2.16) rewrites:

$$
\begin{aligned}
w_i^{n+1} = w_i^n &- \frac{\Delta t}{\Delta x}\left(\frac{h_{i+\frac{1}{2}}}{h_{i+\frac{1}{2}} + z_0} f_{\Delta x}(W_i^n, W_{i+1}^n) - \frac{h_{i-\frac{1}{2}}}{h_{i-\frac{1}{2}} + z_0} f_{\Delta x}(W_{i-1}^n, W_i^n)\right) \\
&+ \frac{g}{2}\frac{\Delta t}{\Delta x}\begin{pmatrix} 0 \\ z_0(h_{i+\frac{1}{2}} - h_{i-\frac{1}{2}}) \end{pmatrix}.
\end{aligned}
\tag{2.17}
$$

By enforcing $z_0 = 0$, we recover the initial homogeneous scheme (2.9). Nevertheless, for $z_0 > 0$ the resulting scheme stays consistent with the expected shallow-water homogeneous system but for additional viscosity when compared to (2.9). The numerical experiments, performed below, will exhibit the efficiency of the scheme and will numerically prove that the bottom location z_0 does not degrade the accuracy of the approximation.

3 Main properties

In this section, we establish the main properties satisfied by the scheme (2.12) or equivalently (2.16). These properties are summarized within the following statements.

Theorem 1 *Let $(w_i^n)_{i\in\mathbb{Z}}$ belongs to $\bar{\Omega}_1$. Assume the updated states given by the scheme (2.13)–(2.16). Then the following properties hold:*

(i) Well-balancing
Assume $u_i^n = 0$ and $h_i^n + z_i = H$ for all $i \in \mathbb{Z}$, where H is a positive given constant. As soon as the numerical flux function satisfies the consistency condition (2.10), the steady state at rest is preserved and we have for all

i in $\mathbb{Z}$:

$$u_i^{n+1} = 0 \qquad \textit{and} \qquad h_i^{n+1} + z_i = H.$$

(ii) Robustness property
Assume the associated homogeneous scheme (2.9) is Ω_1-preserving. Assume that the CFL condition (2.11) holds for all states $(W_i^n)_{i\in\mathbb{Z}}$ as follows:

$$\frac{\Delta t}{\Delta x} \max_{i\in\mathbb{Z}} |\lambda^{\pm}(W_i^n, W_{i+1}^n)| \leq \frac{1}{2}, \tag{3.1}$$

supplemented by the following CFL like restriction (see [37]):

$$\frac{\Delta t}{\Delta x} \Big(\max(0, f_{\Delta x}^h(W_i^n, W_{i+1}^n)) - \min(0, f_{\Delta x}^h(W_{i-1}^n, W_i^n)) \Big) \leq H_i^n, \tag{3.2}$$

then $h_i^{n+1} \geq 0$ for all i in $\mathbb{Z}$.

Let us recall that the usual numerical flux functions (for instance HLL and HLLC schemes [31,51], relaxation schemes [8,16,17,42,35]) satisfy the assumptions stated in the above result.

Moreover, to establish the robustness of the derived method, we need the positiveness of the free surface. As a consequence, at this level, the reference bottom z_0 must be suitably chosen to enforce $H_i^n > 0$ for all i in $\mathbb{Z}$ and $n \in \mathbb{N}$. For instance, for any give topography function Z we can adopt a positive value of z_0 to ensure the required robustness property. The reader is refered to Section 6.1 where the numerical influence of the reference bottom is presented and several choices of z_0 are tested.

Proof. To establish (i), we assume that $u_i^n = 0$ and $h_i^n + z_i = H$. As a consequence, we have $W_i^n = {}^t(H, 0)$ for all $i \in \mathbb{Z}$. Since the numerical flux function $f_{\Delta x}$ is consistent, we get:

$$f_{\Delta x}(W_i^n, W_{i+1}^n) = \begin{pmatrix} 0 \\ \frac{g}{2} H^2 \end{pmatrix},$$

to immediately deduce:

$$\begin{aligned}
&h_i^{n+1} = h_i^n, \\
&(hu)_i^{n+1} = -\frac{\Delta t}{\Delta x} \frac{g}{2} H^2 (X_{i+\frac{1}{2}} - X_{i-\frac{1}{2}}) + \frac{g}{2} \frac{\Delta t}{\Delta x} H_{i-\frac{1}{2}} H_{i+\frac{1}{2}} (X_{i+\frac{1}{2}} - X_{i-\frac{1}{2}}).
\end{aligned}$$

By definition of $H_{i+\frac{1}{2}}$, given by (2.13), we have $H_{i+\frac{1}{2}} = H$ and then we obtain $(hu)_i^{n+1} = 0$ to write $u_i^{n+1} = 0$.

Next, we turn to establish the robustness property. To address such an issue, we follow the arguments introduced by Larrouturrou [37]. Since $X_{i+\frac{1}{2}}$ is given by (2.14), we get the following identity:

$$X_{i+\frac{1}{2}} f^h_{\Delta x}(W^n_i, W^n_{i+1}) = \\ \frac{1}{2}(X^n_i + X^n_{i+1}) f^h_{\Delta x}(W^n_i, W^n_{i+1}) - \frac{1}{2}(X^n_{i+1} - X^n_i)|f^h_{\Delta x}(W^n_i, W^n_{i+1})|.$$

This relation is plugged into the updated water height (2.12) to write:

$$h^{n+1}_i = \alpha X^n_{i-1} + (\tilde{H}^{n+1}_i - \alpha - \beta) X^n_i + \beta X^n_{i+1}, \tag{3.3}$$

where we have set:

$$\alpha = \frac{1}{2}\frac{\Delta t}{\Delta x}\left(f^h_{\Delta x}(W^n_{i-1}, W^n_i) + |f^h_{\Delta x}(W^n_{i-1}, W^n_i)|\right), \tag{3.4}$$

$$\beta = \frac{1}{2}\frac{\Delta t}{\Delta x}\left(-f^h_{\Delta x}(W^n_i, W^n_{i+1}) + |f^h_{\Delta x}(W^n_i, W^n_{i+1})|\right), \tag{3.5}$$

$$\tilde{H}^{n+1}_i = H^n_i - \frac{\Delta t}{\Delta x}\left(f^h_{\Delta x}(W^n_i, W^n_{i+1}) - f^h_{\Delta x}(W^n_{i-1}, W^n_i)\right). \tag{3.6}$$

We easily note that $\alpha \geq 0$, $\beta \geq 0$. Moreover, since we have enforced $H^n_i > 0$ for all $i \in \mathbb{Z}$, we thus get $W^n_i \in \Omega_1$ for all $i \in \mathbb{Z}$. Now, under the CFL condition (3.1), the homogeneous scheme is Ω_1-preserving and then we have $\tilde{H}^{n+1}_i > 0$.

By definition, we have $X^n_i \geq 0$ for all i in $\mathbb{Z}$. As a consequence, the required positiveness of h^{n+1}_i will be established as soon as $\gamma = \tilde{H}^{n+1}_i - \alpha - \beta$ will be proved non-negative. It suffices to evaluate γ according to the sign of both $f^h_{\Delta x}(W^n_{i-1}, W^n_i)$ and $f^h_{\Delta x}(W^n_i, W^n_{i+1})$ to obtain $\gamma \geq 0$ if the additional CFL like condition (3.2) holds. The proof is thus achieved. $\square$

To conclude these proofs of robustness properties, let us remark that h^{n+1}_i satisfies an additional maximum principle given as follows:

$$0 \leq h^{n+1}_i \leq \tilde{H}^{n+1}_i \quad \text{for all } i \in \mathbb{Z}, \tag{3.7}$$

where $\tilde{H}^{n+1}_i$ is defined by (3.6). Indeed, from the relation (3.3) with $\tilde{H}^{n+1}_i > 0$, we can write:

$$\frac{h^{n+1}_i}{\tilde{H}^{n+1}_i} = \frac{\alpha}{\tilde{H}^{n+1}_i} X^n_{i-1} + \frac{\tilde{H}^{n+1}_i - \alpha - \beta}{\tilde{H}^{n+1}_i} X^n_i + \frac{\beta}{\tilde{H}^{n+1}_i} X^n_{i+1},$$

to obtain $\frac{h^{n+1}_i}{\tilde{H}^{n+1}_i}$ as a convex combination of X^n_{i-1}, X^n_i and X^n_{i+1} which belong to $[0, 1]$ and (3.7) is established.

4 Second-order MUSCL extensions

To improve the order of accuracy of the scheme (2.16), we suggest to consider the MUSCL approach [38] (see also [4–6,8,47,36] for related studies) where the numerical flux function $f_{\Delta x}$, initially evaluated with constant cell-centered values, is now computed from limited reconstructed states on each side of the interface.

Over the cell $(x_{i-\frac{1}{2}}, x_{i+\frac{1}{2}})$, we here propose the following reconstruction:

$$
\begin{aligned}
h_i^n(x) &= h_i^n + (x - x_i)s_i^h, \\
(hu)_i^n(x) &= h_i^n u_i^n + (x - x_i)s_i^{hu}, \\
H_i^n(x) &= H_i^n + (x - x_i)s_i^H,
\end{aligned}
$$

where s_i^α denotes any given limited slope for the variable α (for instance a min-mod procedure, see [41,51] to several choices). The reconstruction is assumed to be robust:

$$
h_i^n(x) \geq 0 \quad \text{and} \quad H_i^n(x) > 0 \quad \text{for all } x \in (x_{i-\frac{1}{2}}, x_{i+\frac{1}{2}}),
$$

and constant preserving

$$
s_i^\alpha = 0 \quad \text{if } \alpha_{i-1} = \alpha_i = \alpha_{i+1}.
$$

On each side of an interface $x_{i+\frac{1}{2}}$, we define the inner approximation as follows:

$$
w_i^{n,+} = \begin{pmatrix} h_i^n(x_{i+\frac{1}{2}}) \\ (hu)_i^n(x_{i+\frac{1}{2}}) \end{pmatrix} \quad \text{and} \quad w_{i+1}^{n,-} = \begin{pmatrix} h_{i+1}^n(x_{i+\frac{1}{2}}) \\ (hu)_{i+1}^n(x_{i+\frac{1}{2}}) \end{pmatrix}.
$$

In addition, we set:

$$
(Hu)_i^\pm = \frac{H_i^{n,\pm}(hu)_i^{n,\pm}}{h_i^{n,\pm}},
$$

where $H_i^{n,\pm} = H_i^n(x_{i\pm\frac{1}{2}})$.

For the sake of clarity in the notations, let us define:

$$
W_i^{n,\pm} = \begin{pmatrix} H_i^{n,\pm} \\ (Hu)_i^{n,\pm} \end{pmatrix}.
$$

Once defined the reconstruction, we have to derive the MUSCL scheme. Arguing [5,8,41], let us recall that the MUSCL schemes based on conservative variable reconstructions is nothing but the following average:

$$w_i^{n+1} = \frac{1}{2}\left(w_i^{n+1,-} + w_i^{n+1,+}\right), \tag{4.1}$$

where $w_i^{n+1,-}$ is the first-order updated state on the half-cell $(x_{i-\frac{1}{2}}, x_i)$, for $W_{i-1}^{n,+}$, $W_i^{n,-}$ and $W_i^{n,+}$ at time t^n, defined by:

$$\begin{aligned} w_i^{n+1,-} = w_i^{n,-} - \frac{\Delta t}{\Delta x/2}\Big(&\bar{X}(W_i^{n,-}, W_i^{n,+}, h_i^{n,-}, h_i^{n,+}) f_{\Delta x}(W_i^{n,-}, W_i^{n,+}) - \\ &\bar{X}(W_{i-1}^{n,+}, W_i^{n,-}, h_{i-1}^{n,+}, h_i^{n,-}) f_{\Delta x}(W_{i-1}^{n,+}, W_i^{n,-})\Big) \\ + \frac{g}{2}\frac{\Delta t}{\Delta x}&\begin{pmatrix} 0 \\ \bar{H}(W_{i-1}^{n,+}, W_i^{n,-})\bar{H}(W_i^{n,-}, W_i^{n,+})\times \\ (\bar{X}(W_i^{n,-}, W_i^{n,+}, h_i^{n,-}, h_i^{n,+}) - \bar{X}(W_{i-1}^{n,+}, W_i^{n,-}, h_{i-1}^{n,+}, h_i^{n,-})) \end{pmatrix}, \end{aligned} \tag{4.2}$$

with $\bar{H}(W_L, W_R)$ and $\bar{X}(W_L, W_R, h_L, h_R)$ given by (2.13) and (2.14). Similarly, $w_i^{n+1,+}$ is the first-order updated state on the half-cell $(x_i, x_{i+\frac{1}{2}})$, for $W_i^{n,-}$, $W_i^{n,+}$ and $W_{i+1}^{n,-}$ at time t^n, defined by:

$$\begin{aligned} w_i^{n+1,+} = w_i^{n,+} - \frac{\Delta t}{\Delta x/2}\Big(&\bar{X}(W_i^{n,+}, W_{i+1}^{n,-}, h_i^{n,+}, h_{i+1}^{n,-}) f_{\Delta x}(W_i^{n,+}, W_{i+1}^{n,-}) - \\ &\bar{X}(W_i^{n,-}, W_i^{n,+}, h_i^{n,-}, h_i^{n,+}) f_{\Delta x}(W_i^{n,-}, W_i^{n,+})\Big) \\ + \frac{g}{2}\frac{\Delta t}{\Delta x}&\begin{pmatrix} 0 \\ \bar{H}(W_i^{n,-}, W_i^{n,+})\bar{H}(W_i^{n,+}, W_{i+1}^{n,-})\times \\ (\bar{X}(W_i^{n,+}, W_{i+1}^{n,-}, h_i^{n,+}, h_{i+1}^{n,-}) - \bar{X}(W_i^{n,-}, W_i^{n,+}, h_i^{n,-}, h_i^{n,+})) \end{pmatrix}. \end{aligned} \tag{4.3}$$

After a straightforward computation, the resulting MUSCL scheme reads:

$$\begin{aligned} w_i^{n+1} = w_i^n - \frac{\Delta t}{\Delta x}&\left(\bar{X}_{i+\frac{1}{2}} f_{\Delta x}(W_i^{n,+}, W_{i+1}^{n,-}) - \bar{X}_{i-\frac{1}{2}} f_{\Delta x}(W_{i-1}^{n,+}, W_i^{n,-})\right) \\ &+ \frac{g}{2}\frac{\Delta t}{\Delta x}\left(\bar{H}_i\bar{H}_{i-\frac{1}{2}}(\bar{X}_i - \bar{X}_{i-\frac{1}{2}}) + \bar{H}_i\bar{H}_{i+\frac{1}{2}}(\bar{X}_{i+\frac{1}{2}} - \bar{X}_i)\right), \end{aligned} \tag{4.4}$$

where we have set:

$$\begin{aligned} &\bar{X}_i = \bar{X}(W_i^{n,-}, W_i^{n,+}, h_i^{n,-}, h_i^{n,+}), \qquad &&\bar{X}_{i+\frac{1}{2}} = \bar{X}(W_i^{n,+}, W_{i+1}^{n,-}, h_i^{n,+}, h_{i+1}^{n,-}), \\ &\bar{H}_i = \bar{H}(W_i^{n,-}, W_i^{n,+}), &&\bar{H}_{i+\frac{1}{2}} = \bar{H}(W_i^{n,+}, W_{i+1}^{n,-}). \end{aligned}$$

This second-order accurate scheme preserves the properties stated Theorem 1.

Theorem 2 *Let $(w_i^n)_{i\in\mathbb{Z}}$ belongs to $\bar{\Omega}_1$. Assume the updated states given by the MUSCL scheme (2.13)-(2.14)-(4.4). Then the following properties hold:*

(i) Well-balancing

As soon as the numerical flux function satisfies the consistency condition (2.10), the steady state at rest is preserved.

(ii) Robustness property
Assume the associated homogeneous scheme (2.9) is Ω_1-preserving. Assume that the CFL condition (2.11) holds for the reconstructed states as follows:

$$\frac{\Delta t}{\Delta x} \max_{i\in\mathbb{Z}} \left(|\lambda^{\pm}(W_i^{n,-}, W_i^{n,+})|, |\lambda^{\pm}(W_i^{n,+}, W_{i+1}^{n,-})| \right) \leq \frac{1}{4}, \tag{4.5}$$

supplemented by the following CFL like restriction:

$$\begin{aligned} \frac{\Delta t}{\Delta x} \left(\max(0, f^h_{\Delta x}(W_i^{n,+}, W_{i+1}^{n,-})) - \min(0, f^h_{\Delta x}(W_i^{n,-}, W_i^{n,+})) \right) \leq H_i^{n,+}, \\ \frac{\Delta t}{\Delta x} \left(\max(0, f^h_{\Delta x}(W_i^{n,-}, W_i^{n,+})) - \min(0, f^h_{\Delta x}(W_{i-1}^{n,+}, W_i^{n,-})) \right) \leq H_i^{n,-}, \end{aligned} \tag{4.6}$$

then $h_i^{n+1} \geq 0$ for all i in $\mathbb{Z}$.

Proof. Concerning the well-balance property, we assume $u_i^n = 0$ and $h_i^n + z_i = H$ for all $i \in \mathbb{Z}$. By definition of the reconstruction procedure, we immediately have:

$$(hu)_i^{n,\pm} = 0 \quad \text{and} \quad H_i^{n,\pm} = H,$$

to deduce $(Hu)_i^{n,\pm} = 0$ for all i in $\mathbb{Z}$. Then we have $W_i^{n,\pm} = {}^t(H, 0)$ for all $i \in \mathbb{Z}$ and w_i^{n+1}, defined by (4.4), now reads:

$$\begin{aligned} w_i^{n+1} = w_i^n - \frac{\Delta t}{\Delta x} \left(\bar{X}_{i+\frac{1}{2}} \begin{pmatrix} 0 \\ g\frac{H^2}{2} \end{pmatrix} - \bar{X}_{i-\frac{1}{2}} \begin{pmatrix} 0 \\ g\frac{H^2}{2} \end{pmatrix} \right) \\ + \frac{g}{2} \frac{\Delta t}{\Delta x} \begin{pmatrix} 0 \\ H^2(\bar{X}_i - \bar{X}_{i-\frac{1}{2}}) + H^2(\bar{X}_{i+\frac{1}{2}} - \bar{X}_i) \end{pmatrix}, \end{aligned}$$

to get $w_i^{n+1} = w_i^n$ and the required well-balance property is established.

Next, we prove that the scheme (4.4) is non-negative preserving. Since the updated state w_i^{n+1} satisfies (4.1), the property (ii) holds as soon as both half-updated water heights $h_i^{n+1,+}$ and $h_i^{n+1,-}$ are established non-negative. We focus on $h_i^{n+1,+}$, the proof for $h_i^{n+1,-}$ remains similar.

We note that $w_i^{n+1,+}$ is given by the 3-points first-order scheme (2.16) involving the three states $w_i^{n,-}$, $w_i^{n,+}$ and $w_{i+1}^{n,-}$. Since these three states belong to Ω_1, by applying property (ii) Theorem 1, we immediately deduce that $h_i^{n+1,+}$ is non-negative. The proof is thus completed. □

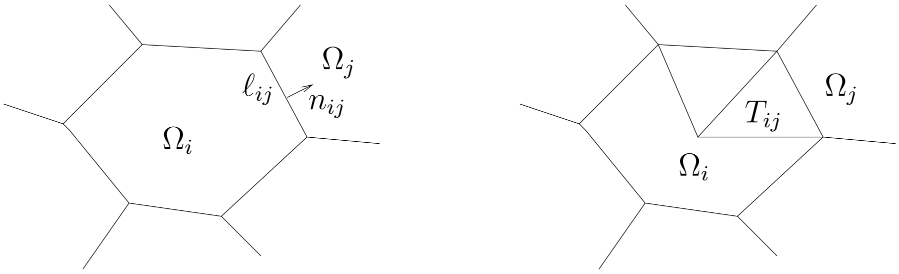

Fig. 1. Cell notations on unstructured meshes.

5 Hydrostatic upwind scheme for 2D unstructured meshes

In this section, we propose to extend the 1D scheme (2.16) in order to consider 2D unstructured meshes. Arguing the same approach than above, the system (1.1) is rewriten involving the free surface $H = h + z$ and the fraction of water $X = h/H$ as follows:

$$\begin{cases} \partial_t h + \partial_x XHu + \partial_y XHv = 0, \\ \partial_t hu + \partial_x \left(X \left(Hu^2 + \frac{g}{2} H^2 \right) - \frac{g}{2} hz \right) + \partial_y XHuv + gh\partial_x z = 0, \\ \partial_t hv + \partial_x XHuv + \partial_y \left(X \left(Hv^2 + \frac{g}{2} H^2 \right) - \frac{g}{2} hz \right) + gh\partial_y z = 0. \end{cases} \tag{5.1}$$

To simplify the notations, we set

$$w = \begin{pmatrix} h \\ hu \\ hv \end{pmatrix}, \quad W = \begin{pmatrix} H \\ Hu \\ Hv \end{pmatrix}, \quad f_x(w) = \begin{pmatrix} hu \\ hu^2 + \frac{g}{2} h^2 \\ huv \end{pmatrix}, \quad f_y(w) = \begin{pmatrix} hv \\ huv \\ hu^2 + \frac{g}{2} h^2 \end{pmatrix}.$$

The system (5.1) thus reads equivalently:

$$\partial_t w + \partial_x (X f_x(W)) + \partial_y (X f_y(W) + \begin{pmatrix} 0 \\ -\frac{g}{2} \nabla(hz) + gh\nabla z \end{pmatrix} = 0. \tag{5.2}$$

In order to discretize this system, the 2D domain is meshed with a set of cells $(\Omega_i)_{i \in \mathbb{Z}}$. For each Ω_i, we denote $\nu(i)$ the set of indexes j such that Ω_j is a neighbor cell. For two neighbor cells Ω_i and Ω_j, we denote ℓ_{ij} the interface and $n_{ij} = {}^t(n_{ij}^x, n_{ij}^y)$ the unit vector normal to the interface ℓ_{ij} and pointing from Ω_i to Ω_j (see figure 1).

Since it will be useful later on, from now on we introduce the triangle T_{ij} made of the interface ℓ_{ij} and the center of Ω_i.

On each cell Ω_i, we denote $w_i^n = {}^t(h_i^n, h_i^n u_i^n, h_i^n v_i^n)$ a constant approximation of the exact solution at time t^n. This approximate state is evolved at time $t^n + \Delta t$ by considering a finite volume scheme.

As soon as the topography is flat, $z = \text{cst}$, we assume known a finite volume method over the considered mesh to approximate the weak solutions of the homogeneous 2D Saint-Venant model which reads as follows:

$$(w^{\text{homo}})_i^{n+1} = w_i^n - \frac{\Delta t}{|\Omega_i|} \sum_{j \in \nu(i)} |\ell_{ij}| \phi(w_i^n, w_j^n, n_{ij}), \tag{5.3}$$

where $\phi(w_L, w_R, n)$ stands for the 2D numerical flux function. As usual, $\phi = {}^t(\phi^h, \phi^{hu}, \phi^{hv})$ can be derived from the 1D scheme (2.9) arguing some rotational invariance properties (for instance, see [5,25]). Of course, distinct approaches can be considered to derive 2D scheme in the form (5.3).

We impose the numerical flux to be consistent:

$$\phi(w, w, n) = (f_x(w) \ f_y(w)) \cdot n. \tag{5.4}$$

Before we derive the scheme with non-flat topography, let us recall the following statement (for instance, see [5]) since it will be useful in the sequel:

Lemma 3 *The finite volume scheme (5.3) reads as a convex combination of 1D schemes stated at each interface ℓ_{ij} direction:*

$$(w^{\text{homo}})_i^{n+1} = \sum_{j \in \nu(i)} \frac{|T_{ij}|}{|\Omega_i|} \tilde{w}_{ij}^{n+1}, \tag{5.5}$$

where we have set

$$\tilde{w}_{ij}^{n+1} = w_i^n - \frac{\Delta t}{|T_{ij}|} |\ell_{ij}| \left(\phi(w_i^n, w_j^n, n_{ij}) - \phi(w_i^n, w_i^n, n_{ij}) \right). \tag{5.6}$$

We skip the proof of this easy result which directly comes from the following discrete Green formula:

$$\sum_{j \in \nu(i)} |\ell_{ij}| \phi(w_i^n, w_i^n, n_{ij}) = 0.$$

With some benefits, we argue the above decomposition of the 2D finite volume scheme to substitute the homogeneous 1D scheme (5.6) by the modification coming from (2.12) to discretize the topography source term. As a consequence, we suggest the following formula:

$$\begin{aligned}
\tilde{h}_{ij}^{n+1} &= h_i^n - \frac{\Delta t}{|T_{ij}|}|\ell_{ij}|(X_{ij}\phi^h(W_i^n, W_j^n, n_{ij}) - X_{ii}\phi^h(W_i^n, W_i^n, n_{ij})),\\
(\tilde{hu})_{ij}^{n+1} &=(hu)_i^n - \frac{\Delta t}{|T_{ij}|}|\ell_{ij}| \left(X_{ij}\phi^{hu}(W_i^n, W_j^n, n_{ij}) - X_{ii}\phi^{hu}(W_i^n, W_i^n, n_{ij})\right)\\
&\quad + \frac{g}{2}\frac{\Delta t}{|T_{ij}|}|\ell_{ij}|(h_{ij}z_{ij} - h_{ii}z_{ii})n_{ij}^x - g\frac{\Delta t}{|T_{ij}|}|\ell_{ij}|\frac{h_{ii}+h_{ij}}{2}(z_{ij} - z_{ii})n_{ij}^x,\\
(\tilde{hv})_{ij}^{n+1} &=(hv)_i^n - \frac{\Delta t}{|T_{ij}|}|\ell_{ij}| \left(X_{ij}\phi^{hv}(W_i^n, W_j^n, n_{ij}) - X_{ii}\phi^{hv}(W_i^n, W_i^n, n_{ij})\right)\\
&\quad + \frac{g}{2}\frac{\Delta t}{|T_{ij}|}|\ell_{ij}|(h_{ij}z_{ij} - h_{ii}z_{ii})n_{ij}^y - g\frac{\Delta t}{|T_{ij}|}|\ell_{ij}|\frac{h_{ii}+h_{ij}}{2}(z_{ij} - z_{ii})n_{ij}^y,
\end{aligned}$$

where we have set

$$X_{ij} = \bar{X}(W_i^n, W_j^n, h_i^n, h_j^n, n_{ij}) \quad \text{and} \quad H_{ij} = \bar{H}(W_i^n, W_j^n, n_{ij}), \tag{5.7}$$

$$h_{ij} = H_{ij}X_{ij} \quad \text{and} \quad z_{ij} = H_{ij}(1 - X_{ij}), \tag{5.8}$$

with

$$\bar{H}(W_L, W_R, n) = \begin{cases} H_L & \text{if } \phi^h(W_L, W_R, n) > 0,\\ H_R & \text{otherwise,}\end{cases} \tag{5.9}$$

$$\bar{X}(W_L, W_R, h_L, h_R, n) = \begin{cases} X_L = \frac{h_L}{H_L} & \text{if } \phi^h(W_L, W_R, n) > 0,\\ X_R = \frac{h_R}{H_R} & \text{otherwise.}\end{cases} \tag{5.10}$$

From (5.5), the updated state at time t^{n+1} reads:

$$\begin{aligned}
w_i^{n+1} = w_i^n &- \frac{\Delta t}{|\Omega_i|}\sum_{j\in\nu(i)} |\ell_{ij}|X_{ij}\phi(W_i^n, W_j^n, n_{ij})\\
&+ \frac{g}{2}\frac{\Delta t}{|\Omega_i|}\sum_{j\in\nu(i)} |\ell_{ij}|\begin{pmatrix}0\\ h_{ij}z_{ij}n_{ij}\end{pmatrix}\\
&- g\frac{\Delta t}{|\Omega_i|}\sum_{j\in\nu(i)} |\ell_{ij}|\begin{pmatrix}0\\ \frac{h_{ii}+h_{ij}}{2}(z_{ij} - z_{ii})n_{ij}\end{pmatrix}
\end{aligned}$$

By involving a straightforward computation, we obviously obtain the following sequence of equalities:

$$\begin{aligned}\sum_{j\in\nu(i)} |\ell_{ij}|(h_{ij}z_{ij} - (h_{ii}+h_{ij})(z_{ij}-z_{ii}))n_{ij} &= \sum_{j\in\nu(i)} |\ell_{ij}|(h_{ij}z_{ii} - h_{ii}z_{ij})n_{ij}, \\ &= \sum_{j\in\nu(i)} |\ell_{ij}|(H_{ij}X_{ij}H_{ii}(1-X_{ii}) - H_{ii}X_{ii}H_{ij}(1-X_{ij}))n_{ij}, \\ &= \sum_{j\in\nu(i)} |\ell_{ij}|H_{ii}H_{ij}(X_{ij}-X_{ii})n_{ij}.\end{aligned}$$

Hence, we deduce the useful and non-expensive formulation of the 2D scheme for varying topography:

$$\begin{aligned} w_i^{n+1} = w_i^n &- \frac{\Delta t}{|\Omega_i|}\sum_{j\in\nu(i)} |\ell_{ij}|X_{ij}\phi(W_i^n, W_j^n, n_{ij}) \\ &+ \frac{g}{2}\frac{\Delta t}{|\Omega_i|}\sum_{j\in\nu(i)} |\ell_{ij}| \begin{pmatrix} 0 \\ H_{ii}H_{ij}(X_{ij}-X_{ii})n_{ij}\end{pmatrix}\end{aligned} \tag{5.11}$$

To conclude the derivation of the 2D scheme on unstructured meshes, we establish both well-balanced and non-negative preserving properties.

Theorem 4 *Let $(w_i^n)_{i\in\mathbb{Z}}$ belongs to $\bar{\Omega}_2$. Assume the updated states given by the scheme (5.11). Then the following properties hold:*

(i) Well-balancing
As soon as the numerical flux function satisfies the consistency condition (5.4), the steady state at rest is preserved.

(ii) Robustness property
Assume the associated homogeneous scheme (5.3) is Ω_2-preserving. Assume that the following 2D CFL condition holds:

$$\Delta t \max_{i\in\mathbb{Z},\ j\in\nu(i)} \frac{|\ell_{ij}|}{|T_{ij}|}|\lambda^{\pm}(W_i^n, W_j^n)| \leq \frac{1}{2}, \tag{5.12}$$

supplemented by the following CFL like restriction:

$$\Delta t\frac{|\ell_{ij}|}{|T_{ij}|}\Big(\max(0,\phi^h(W_i^n, W_j^n, n_{ij})) - \min(0, \phi^h(W_i^n, W_i^n, n_{ij}))\Big) \leq H_i^n, \tag{5.13}$$

then $h_i^{n+1}\geq 0$ for all i in $\mathbb{Z}$.

Once again we emphasize that the usual numerical flux functions (for instance HLL, HLLC, relaxation schemes) satisfy the assumptions imposed in this result.

Proof. We assume that $u_i^n = v_i^n = 0$ and $h_i^n + z_i = H_i^n = H$, where H is a given constant. As a consequence, we have $W_i^n = {}^t(H, 0)$ for all $i \in \mathbb{Z}$ and $H_{ij} = H$ for all $(i, j) \in \mathbb{Z} \times (\{i\} \cup \nu(i))$. Next, by involving the consistency property, we get:

$$\phi(W, W, n) = g\frac{H^2}{2}\begin{pmatrix} 0 \\ n \end{pmatrix},$$

to write (5.11) as follows:

$$\begin{aligned} w_i^{n+1} &= w_i^n - \frac{\Delta t}{|\Omega_i|}\sum_{j\in\nu(i)} |\ell_{ij}|X_{ij}\begin{pmatrix} 0 \\ \frac{g}{2}H^2 n_{ij} \end{pmatrix} \\ &\qquad + \frac{g}{2}\frac{\Delta t}{|\Omega_i|}\begin{pmatrix} 0 \\ \sum_{j\in\nu(i)} |\ell_{ij}|H^2(X_{ij} - X_{ii})n_{ij} \end{pmatrix}, \\ &= w_i^n. \end{aligned}$$

Hence, the scheme is well-balanced since we have $H_i^{n+1} = h_i^{n+1} + z_i = H$ and $(hu)_i^{n+1} = (hv)_i^n = 0$.

Now, we turn considering the non-negativeness of h_i^{n+1}. To address such an issue, we consider the formulation (5.5)-(5.6) of the 2D finite volume scheme (5.11). As a consequence, the proof is achieved as soon as we establish $\tilde{h}_{ij}^{n+1} \geq 0$ where

$$\tilde{h}_{ij}^{n+1} = h_i^n - \frac{\Delta t}{|T_{ij}|}|\ell_{ij}|(X_{ij}\phi^h(W_i^n, W_j^n, n_{ij}) - X_{ii}\phi^h(W_i^n, W_i^n, n_{ij})).$$

Similarly to the 1D case, arguing the definition of X_{ij} given by (5.7)-(5.10), the above intermediate water height rewrites:

$$\tilde{h}_{ij}^{n+1} = \alpha X_i^n + (\tilde{H}_{ij}^{n+1} - \alpha - \beta)X_i^n + \beta X_j^n,$$

where

$$\begin{aligned} \alpha &= \frac{1}{2}\frac{\Delta t}{|T_{ij}}|\ell_{ij}|\left(\phi^h(W_i^n, W_i^n, n_{ij}) + |\phi^h(W_i^n, W_i^n, n_{ij})|\right) \geq 0, \\ \beta &= \frac{1}{2}\frac{\Delta t}{|T_{ij}}|\ell_{ij}|\left(-\phi^h(W_i^n, W_j^n, n_{ij}) + |\phi^h(W_i^n, W_j^n, n_{ij})|\right) \geq 0, \\ \tilde{H}_{ij}^{n+1} &= H_i^n - \frac{\Delta t}{|T_{ij}}|\ell_{ij}|\left(\phi^h(W_i^n, W_j^n, n_{ij}) - \phi^h(W_i^n, W_i^n, n_{ij})\right). \end{aligned}$$

Involving the CFL condition (5.12) and (5.13), we immediately obtain $\tilde{H}_{ij}^{n+1} - \alpha - \beta \geq 0$ which implies $\tilde{h}_{ij}^{n+1} \geq 0$. As a consequence, we deduce h_i^{n+1} is non-negative and the proof is completed. $\square$

6 Numerical experiments

The present section is devoted to present several numerical experiments in order to illustrate the interest of the proposed hydrostatic upwind scheme. First, we perform 1D simulations to validate the scheme and exhibit its main properties. Next, 2D approximations are made on unstructured meshes to simulate experiments of physical interest. The numerical tests are performed by involving numerical flux function given by the HLLC scheme [52] and the VFRoe method [21,23,22]. The HLLC is known to satisfy all the assumptions required in Theorem 1, 2 and 4. Concerning the VFRoe flux function, after [7], a relevant CFL condition can be exhibited to satisfy the expected robustness properties.

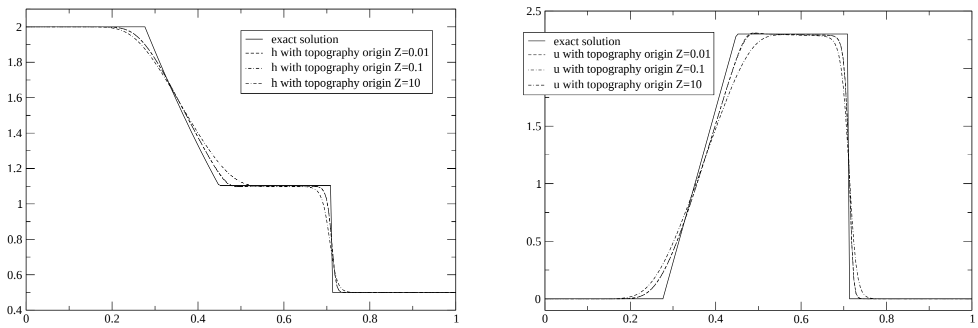

Fig. 2. First-order wet dam-break.

6.1 Dam-break approximations

To validate the suggested scheme, we propose to simulate a dam break on wet area. The grid is made of 200 cells and the adopted numerical flux function is given by the well-known HLLC scheme (see [52]). The initial data is given as follows:

$$h(x,0) = \begin{cases} 2 & \text{if } x < 0, \\ 1/2 & \text{if } x > 0, \end{cases} \qquad \text{and} \qquad u(x,0) = 0.$$

It is essential to recall that our procedure depends on the choice of the bottom origin (see (2.17)). As a consequence, we here show the numerical results obtained by considering several choices of this origin of topography; respectively $z_0 = 0.01$, $z_0 = 0.1$ and $z_0 = 10$. Figure 2 concerns the first-order numerical approximations. We note good agreement with the exact solution for all bottom origins despite an increasing of the numerical viscosity as the adopted origin grows.

Figure 3 is devoted to exhibit the behavior of the method when adopting a second-order MUSCL reconstruction with a standard minmod inner recon-

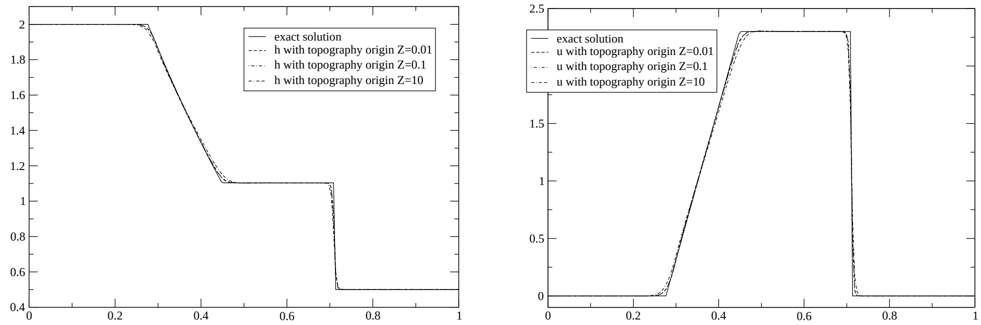

Fig. 3. Second-order wet dam-break.

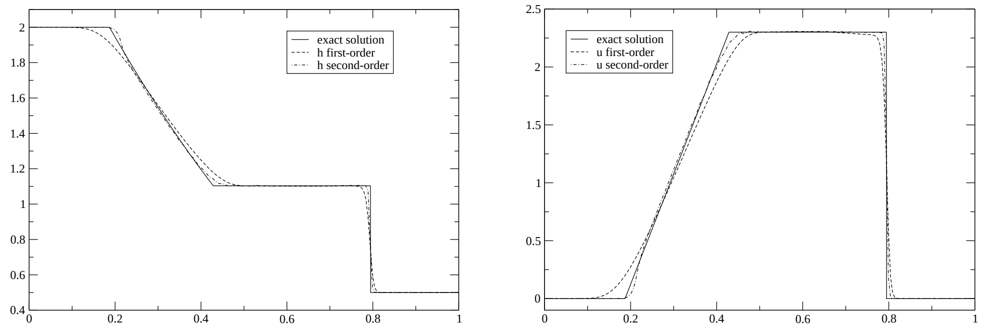

Fig. 4. Wet dam-break with a time variable topography origin.

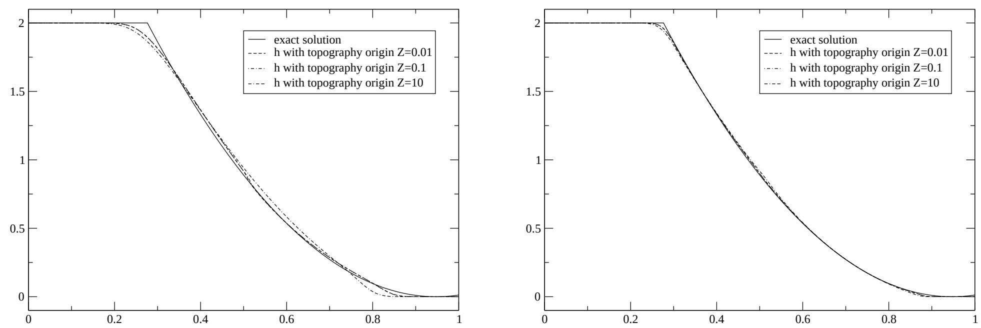

Fig. 5. First and second-order dam-break on dry area: water height.

struction. As expected we obtain more accurate approximate solution. Once again, we remark that the topography does not affect the consistency of the method.

From now on, let us underline that the choice of the topography origin can be made locally in time. To assert this remark, we propose to define the topography origin as a function of time as follows:

$$z_0(t) = \sin\left(2\pi \frac{t}{0.07}\right),$$

and to consider the above dam-break. The obtain result (first- and second-order) are displayed figure 4. Once again, we do not remark some influence of the choice of z_0.

We complete these dam-break simulations by performing a dam-break over dry area. Once again we choose a topography origin given by $z_0 = 0.01$, $z_0 = 0.1$ and $z_0 = 10$. In Figure 5, we present the water height obtained with first and second-order hydrostatic upwind scheme. The approximations stay in good agreement with the exact solution and the role played by the topography origin remains negligible.

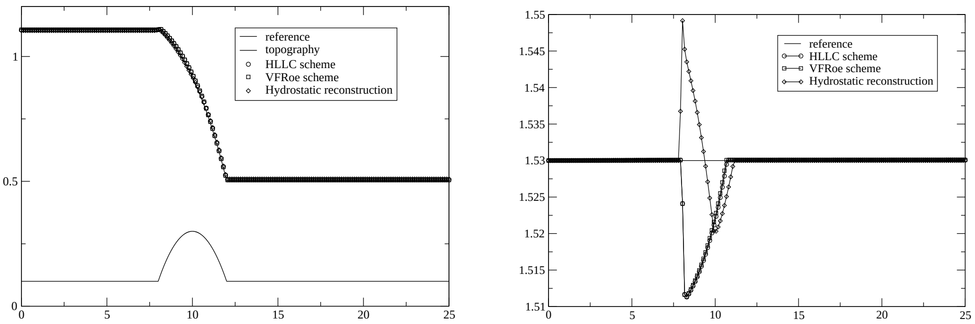

Fig. 6. Trasnscritical flow without shock: comparison between first-order hydrostatic upwind with HLLC and VFRoe numerical flux function and first-order well-known hydrostatic reconstruction with HLLC numerical flux function (left: water height, right: discharge).

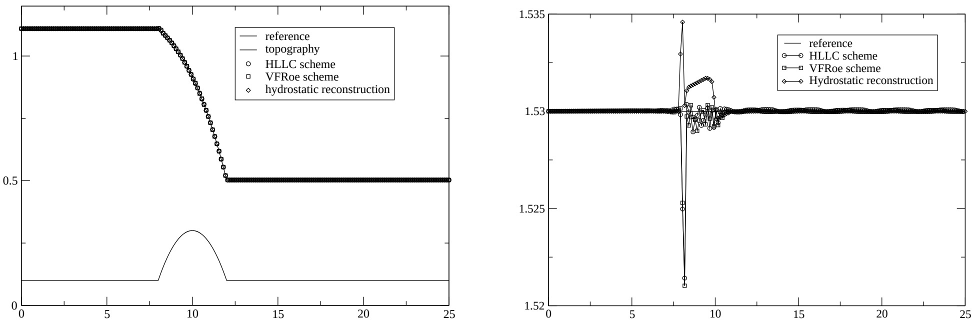

Fig. 7. Trasnscritical flow without shock: comparison between second-order hydrostatic upwind with HLLC and VFRoe numerical flux function and second-order well-known hydrostatic reconstruction with HLLC numerical flux function (left: water height, right: discharge).

6.2 *Subcritical and transcritical flow over a bump*

We turn to consider the flow over a bump as introduced in [27,28]. The domain is $[0, 25]$ and the topography admits a bump as follows:

$$z(x) = \begin{cases} 0.3 - 0.05(x-10)^2 & \text{if } 8 < x < 12, \\ 0.1 & \text{otherwise.} \end{cases}$$

Form now on, let us note that we have fixed the topography origin by $z_0 = 0.1$. The mesh is made of 200 cells. With some benefit, we use these benchmarks

Cells	Hydrostatic upwind		Hydrostatic reconstruction	
	L^1-error	L^2-error	L^1-error	L^2-error
128	5.0150E-2	1.0970E-3	3.8790E-2	6.0654E-4
256	2.4783E-2	2.7635E-4	1.8246E-2	1.4177E-4
512	1.2311E-2	6.9202E-5	8.8773E-3	3.4424E-5
1024	6.1333E-3	1.7315E-5	4.3800E-3	8.5075E-6
2048	3.0608E-3	4.3363E-6	2.1765E-3	2.1252E-6

Table 1
Discharge error for the first-order approximation of the transcritical flow without shock.

to evaluate the influence of the numerical flux function. We will consider the HLLC and VFRoe flux functions.

The first test concerns a transcritical flow without shock. To perform this numerical experiment, the initial data is given by:

$$h(x,0)+z(x)=0.66 \quad \text{and} \quad h(x,0)u(x,0)=0.$$

The boundary conditions are $h(0,t)u(0,t)=1.53$ and $h(25,t)=0.66$. In figure 6, we present the results obtained by considering the first-order suggested hydrostatic upwind with both HLLC and VFRoe numerical flux functions and the first-order hydrostatic reconstruction with HLLC numerical flux functions.

We note a very good agreement with the exact solution. Concerning the discharge, which should be constant in this test, we note that the numerical flux function does not affect the behavior of the numerical approximation.

Similarly, figure 7 shows second-order accurate approximations. We note that the discharge approximation is clearly better. In the tables 1 and 2, we give the discharge errors.

The second test is devoted to a transcritical flow with a shock. The initial data is now fixed as follows:

$$h(x,0)+z(x)=0.33 \quad \text{and} \quad h(x,0)u(x,0)=0,$$

while the boundary conditions are given by $h(0,t)u(0,t)=0.18$ and $h(25,t)=0.33$. In figure 8, we present the results obtained by considering a first-order hydrostatic upwind with both HLLC and VFRoe numerical flux functions and first-order classical hydrostatic reconstruction with HLLC numerical flux functions.

In the tables 3 and 4, we give the discharge errors.

Cells	Hydrostatic upwind		Hydrostatic reconstruction	
	L^1-error	L^2-error	L^1-error	L^2-error
128	6.5096E-3	5.0379E-5	8.6804E-3	3.6090E-5
256	3.3271E-3	6.8732E-6	2.3566E-3	3.5530E-6
512	1.1855E-3	7.7995E-7	6.3573E-4	3.8020E-7
1024	4.2468E-4	1.4760E-7	2.0375E-4	5.4210E-8
2048	1.1162E-4	3.6429E-8	6.3717E-5	1.2427E-8

Table 2
Discharge error for the second-order approximation of the transcritical flow without shock.

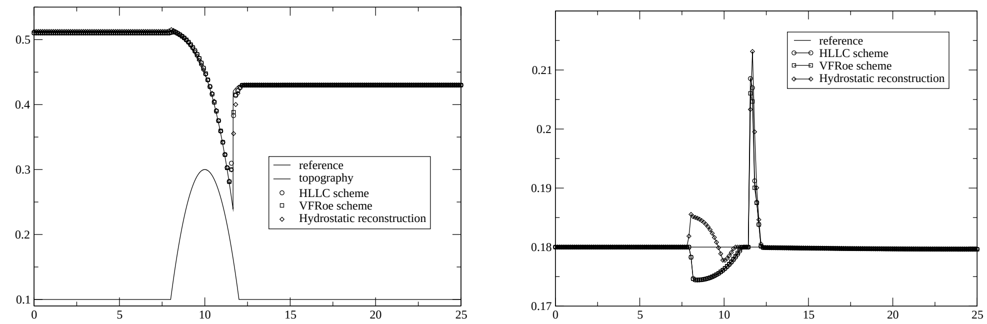

Fig. 8. Trasnscritical flow with shock: comparison between first-order hydrostatic upwind with HLLC and VFRoe numerical flux function and first-order hydrostatic reconstruction with HLLC numerical flux function (left: water height, right: discharge).

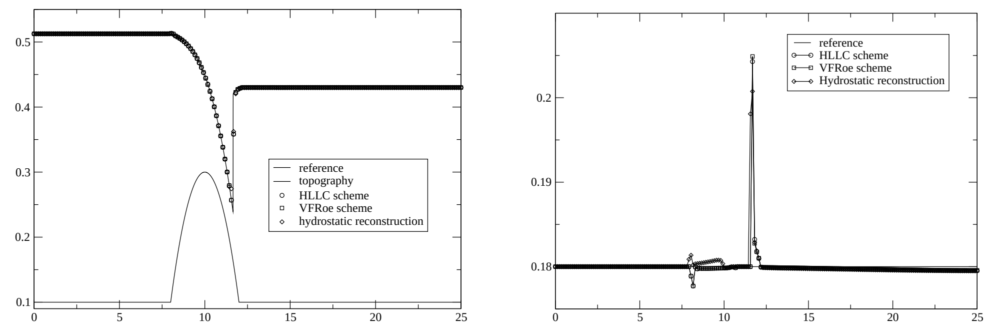

Fig. 9. Trasnscritical flow with shock: comparison between second-order proposed hydrostatic upwind with HLLC and VFRoe numerical flux function and second-order classical hydrostatic reconstruction with HLLC numerical flux function (left: water height, right: discharge).

In the last test, we simulate a subcritical flow over the bump. To address such an issue, we consider the following initial data:

$$h(x,0) + z(x) = 2 \quad \text{and} \quad h(x,0)u(x,0) = 0.$$

We have $h(0,t)u(0,t) = 4.42$ and $h(25,t) = 2$ as boundary conditions. In fig-

Cells	Hydrostatic upwind		Hydrostatic reconstruction	
	L^1-error	L^2-error	L^1-error	L^2-error
128	3.6971E-2	4.8146E-4	3.1715E-2	5.0701E-4
256	2.0810E-2	2.0047E-4	1.8190E-2	2.2270E-4
512	1.2505E-2	8.6188E-5	1.1277E-2	9.9696E-5
1024	8.3797E-3	4.2292E-5	7.7002E-3	4.8074E-5
2048	6.2847E-3	2.0594E-5	5.9886E-3	2.3733E-5

Table 3
Discharge error for the first-order approximation of the transcritical flow with shock.

Cells	Hydrostatic upwind		Hydrostatic reconstruction	
	L^1-error	L^2-error	L^1-error	L^2-error
128	L1 1.7241E-2	3.9508E-4	1.7238E-2	2.9985E-4
256	7.6751E-3	7.3352E-5	8.6884E-3	6.1706E-5
512	6.6427E-3	7.6694E-5	6.5501E-3	6.1101E-5
1024	5.0403E-3	2.0213E-5	5.2237E-3	1.6692E-5
2048	4.8286E-3	1.9016E-5	4.8530E-3	1.7486E-5

Table 4
Discharge error for the second-order approximation of the transcritical flow with shock.

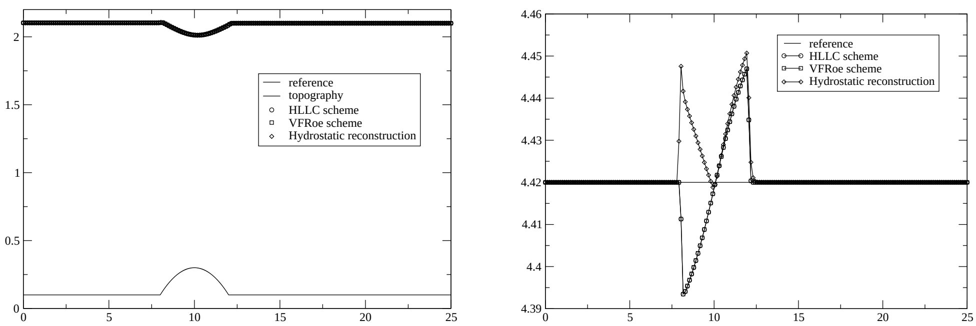

Fig. 10. Subcritical flow: comparison between first-order hydrostatic upwind with HLLC and VFRoe numerical flux function and first-order usual hydrostatic reconstruction with HLLC numerical flux function (left: water height, right: discharge).

ures 10 and 11, we present the results obtained by considering both first and second-order hydrostatic upwind with both HLLC and VFRoe numerical flux functions and both first and second-order well-known hydrostatic reconstruction with HLLC numerical flux functions.

Once again, we note a fairly good agreement between approximate solutions and exact solutions. This is confirmed by the tables 5 and 6 concerning the

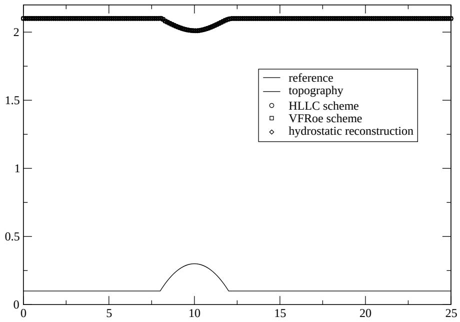

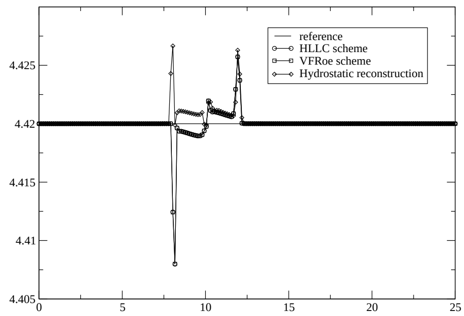

Fig. 11. Subcritical flow: comparison between second-order presented hydrostatic upwind with HLLC and VFRoe numerical flux function and second-order usual hydrostatic reconstruction with HLLC numerical flux function (left: water height, right: discharge).

Cells	Hydrostatic upwind		Hydrostatic reconstruction	
	L^1-error	L^2-error	L^1-error	L^2-error
128	9.8131E-2	2.9477E-3	9.3391E-2	2.8403E-3
256	4.8934E-2	7.3867E-4	4.6436E-2	7.1341E-4
512	2.4444E-2	1.8714E-4	2.3248E-2	1.8072E-4
1024	1.2238E-2	4.7173E-5	1.1667E-2	4.5581E-5
2048	6.1438E-3	1.1809E-5	5.8706E-3	1.1436E-5

Table 5
Discharge error for the first-order approximation of the subcritical flow.

Cells	Hydrostatic upwind		Hydrostatic reconstruction	
	L^1-error	L^2-error	L^1-error	L^2-error
128	1.6926E-2	1.4799E-4	1.5134E-2	8.2362E-5
256	4.3830E-3	1.6440E-5	4.0907E-3	9.2650E-6
512	1.1464E-3	2.0479E-6	1.1275E-3	1.1523E-6
1024	3.4185E-4	3.7613E-7	3.4257E-4	1.8247E-7
2048	1.3401E-4	8.6144E-8	1.3857E-4	3.4296E-8

Table 6
Discharge error for the second-order approximation of the transcritical flow.

discharge errors.

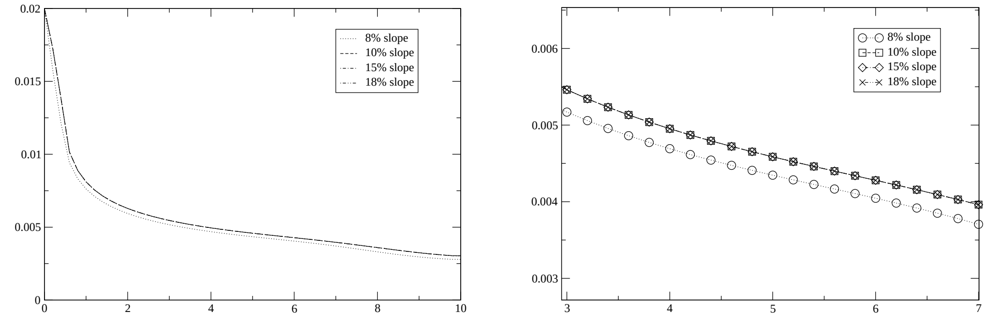

Fig. 12. Streaming simulation by well-known hydrostatic reconstruction with first-order HLLC numerical flux function.

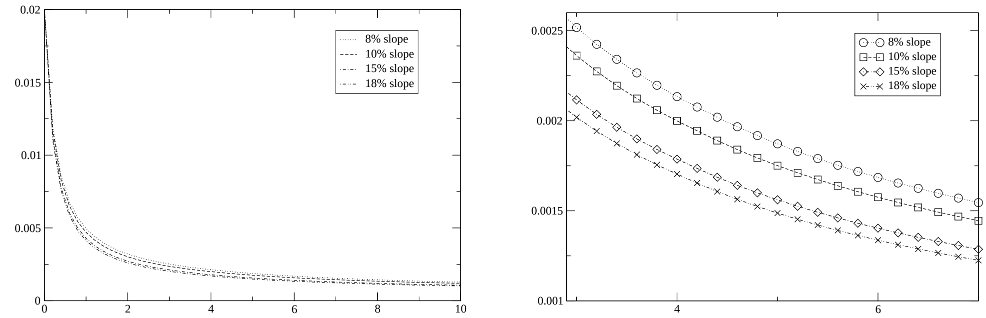

Fig. 13. Streaming simulation by the derived hydrostatic upwind with first-order HLLC numerical flux function and a topography origin fixed to $z_0 = 0.1$.

6.3 Streaming failure

We here examine the problem of the streaming over a bottom made of a constant slope. The domain is $[0, 25]$ and we just impose an imput data given by

$$h(0, t) = 0.02 \text{ m} \quad \text{and} \quad (hu)(0, t) = 0.0025 \text{ m}^2/\text{s}.$$

By increasing the slope of the topography, we expect that the water height in the domain decreases. This benchmark was introduced by Delestre in [18] to exhibit a failure of the classical hydrostatic reconstruction. Indeed, considering a coarse mesh, here made of 50 cells, the hydrostatic reconstruction technique is not able to restore the suitable water height behavior. In figure 12, we present the numerical results obtained when the topography slope varies from 8% to 18%. We note that the water height increases for slopes from 8% to 10%. Next, we obtain the same results for slope from 10% to 18%. This shows that the hydrostatic reconstruction fails to simulate such streaming behavior.

Let us underline that this hydrostatic reconstruction failure seems to be corrected by considering small enough Δx or by involving second-order extensions (see [18]).

Now, figure 13, we have the numerical results obtained by the presented hydrostatic upwind scheme. The expected behavior of h is obtained with the same coarse grid.

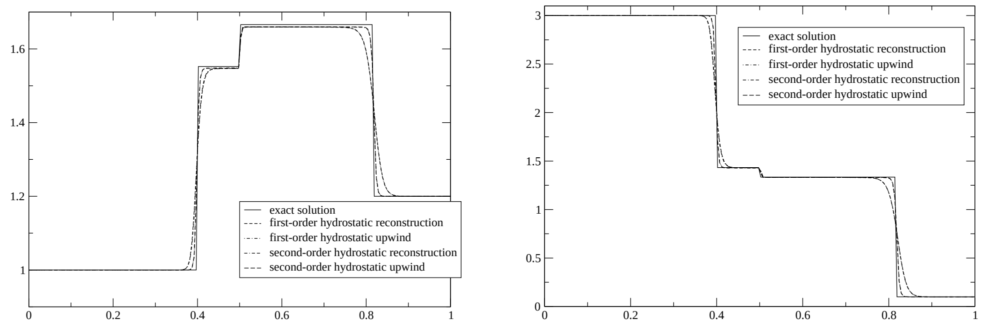

Fig. 14. Discontinuous topography: first resonant test with unique solution (left: water height, right: water velocity).

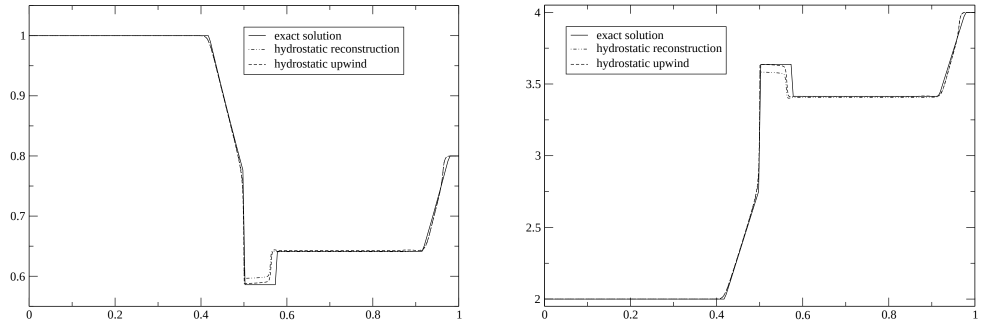

Fig. 15. Discontinuous topography: second resonant test with unique solution (left: water height, right: water velocity).

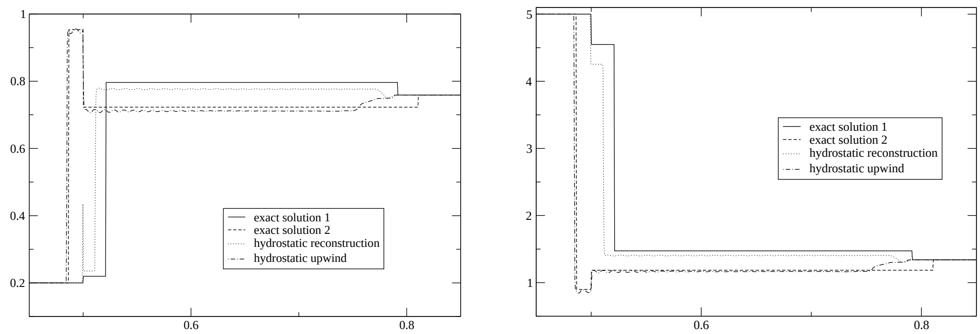

Fig. 16. Discontinuous topography: resonant regime with multiple solutions (left: water height, right: water velocity).

6.4 Discontinuous topography with resonant regime

We consider resonant regimes coming from a discontinuous topography. The associated Riemann problem was studied in [39,40] where exact solutions are proposed. Let us recall that resonant regime may involve unique or multiple solutions. The first simulation is given by the following Riemann initial data:

$$h(x,0) = \begin{cases} 1 & \text{if } x < 0.5, \\ 1.2 & \text{otherwise,} \end{cases} \quad \text{and} \quad u(x,0) = \begin{cases} 3 & \text{if } x < 0.5, \\ 0.1 & \text{otherwise,} \end{cases}$$

while the discontinuous topography is defined as follows:

$$z(x) = \begin{cases} 1.1 & \text{if } x < 0.5, \\ 1 & \text{otherwise.} \end{cases}$$

In figure 14 we present the numerical results obtained with both hydrostatic reconstruction and hydrostatic upwind approaches with first and second-order. Here, we have considered 200 cells and we note a very good comparison with the exact solution.

The second resonant test concerns a more difficult experiment presented in [40] where a standard Godunov scheme cannot restore the required solution. The topography stays the same:

$$z(x) = \begin{cases} 1.1 & \text{if } x < 0.5, \\ 1 & \text{otherwise.} \end{cases}$$

The initial data is now given by

$$h(x,0) = \begin{cases} 1 & \text{if } x < 0.5, \\ 0.8 & \text{otherwise,} \end{cases} \quad \text{and} \quad u(x,0) = \begin{cases} 2 & \text{if } x < 0.5, \\ 4 & \text{otherwise.} \end{cases}$$

In figure 15 the numerical approximations obtained by both hydrostatic reconstruction and upwind approaches are displayed. The adopted numerical flux function is given by the HLLC procedure and we have considered a fine mesh made of 800 cells. The general structure solution is fairly good captured by both techniques and we obtain a good resolution of the composite wave. However and despite a fine mesh, the hydrostatic scheme presents some difficulties to converge to the expected second intermediate state.

The last resonant simulation is devoted to the case of multiple solutions [40]. Such multiple solution problem is obtained by considering the following initial data:

$$h(x,0) = \begin{cases} 0.2 & \text{if } x < 0.5, \\ 0.75904946 & \text{otherwise,} \end{cases} \quad u(x,0) = \begin{cases} 5 & \text{if } x < 0.5, \\ 1.3410741 & \text{otherwise.} \end{cases}$$

The discontinuous topography is defined as follows:

$$z(x) = \begin{cases} 1 & \text{if } x < 0.5, \\ 1.2 & \text{otherwise.} \end{cases}$$

Three distinct solutions satisfy the problem under consideration. The first one is just the stationary solution made of the initial data for all time $t > 0$. The two other admissible solutions are made of three discontinuities; namely two shock waves and a stationary contact discontinuity associated to the topography discontinuity. Both exact solutions are presented in figure 16.

In order to focus on converged results, we fix mesh with 2000 cells. We note that the usual hydrostatic reconstruction does not converge to one of the exact solutions but stays near from the first exact solution. Reversely, the hydrostatic upwind scheme is near from the second exact solution. In fact, we remark that the obtained numerical result is relevant to approximate the first two discontinuities while an error occurs to correctly capture the second intermediate state.

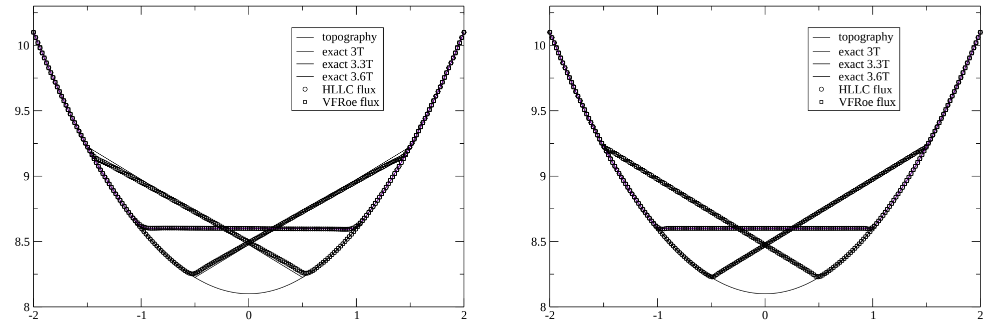

Fig. 17. Thaker's test: water height at time $t = 3T$, $t = 3.3T$ and $t = 3.6T$ (left: first-order, right: second-order).

6.5 *Thacker's test*

The goal of this numerical experiment is to evaluate the scheme to restore relevant dry/wet transition (see [50]). The computational domain is $[-2, 2]$ and the topography is given as follows:

$$z(x) = \frac{1}{2}(x^2 - 1).$$

The initial data is defined by $u(x, 0) = 0$ and

$$h(x,0) = \begin{cases} \frac{1}{2}\left(1 - (x + \frac{1}{2})^2\right) & \text{if } -\frac{3}{2} < x < -\frac{1}{2}, \\ 0 & \text{otherwise.} \end{cases}$$

The analytical solution is T-periodic, with $T = \pi\sqrt{g}$. The exact water height and velocity are given by

$$h(x,t) = \begin{cases} \frac{1}{2}\left(1 - (x + \frac{1}{2}\cos(t\sqrt{g})^2\right) \\ \qquad\qquad \text{if } -\frac{1}{2}\cos(t\sqrt{g}) - 1 < x < -\frac{1}{2}\cos(t\sqrt{g}) + 1, \\ 0 \qquad\qquad \text{otherwise,} \end{cases}$$

$$u(x,t) = \begin{cases} \frac{1}{2}\sqrt{g}\cos(t\sqrt{g}) & \text{if } -\frac{1}{2}\cos(t\sqrt{g}) - 1 < x < -\frac{1}{2}\cos(t\sqrt{g}) + 1, \\ 0 & \text{otherwise.} \end{cases}$$

The obtained numerical results are displayed figure 17. We note a small lost of accuracy in time with the first-order schemes, it is corrected by the second-order MUSCL extension.

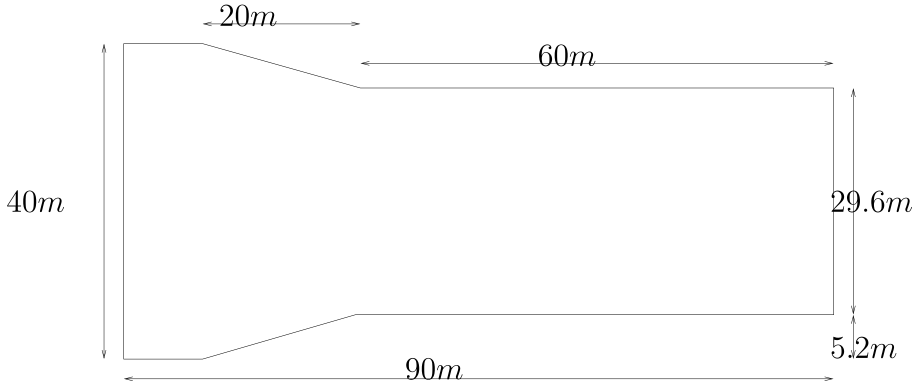

Fig. 18. Geometry of the canal with variable length.

6.6 *Two-dimensional experiments*

We here perform 2D numerical simulations on unstructured meshes. The first test we consider (for instance, see [15]) concerns a channel with symmetric complex geometry. The objective of this experiment is to approximate sophisticated hydraulic jumps.

As presented figure 18, the channel length is $90m$ and it is $40m$ input length. The length channel reduces and the output length is $29.6m$. Here, we have adopted an unstructured mesh made of 32811 nodes and 64923 triangles. The input boundary condition is fixed as follows: the water height is $1m$ while the velocity is $7.9ms^{-1}$ in the normal direction to the boundary. In figure 19, we show the obtained approximate water height at the stationary regime when considering a flat bottom. We note that the sequence of shock waves are well-captured.

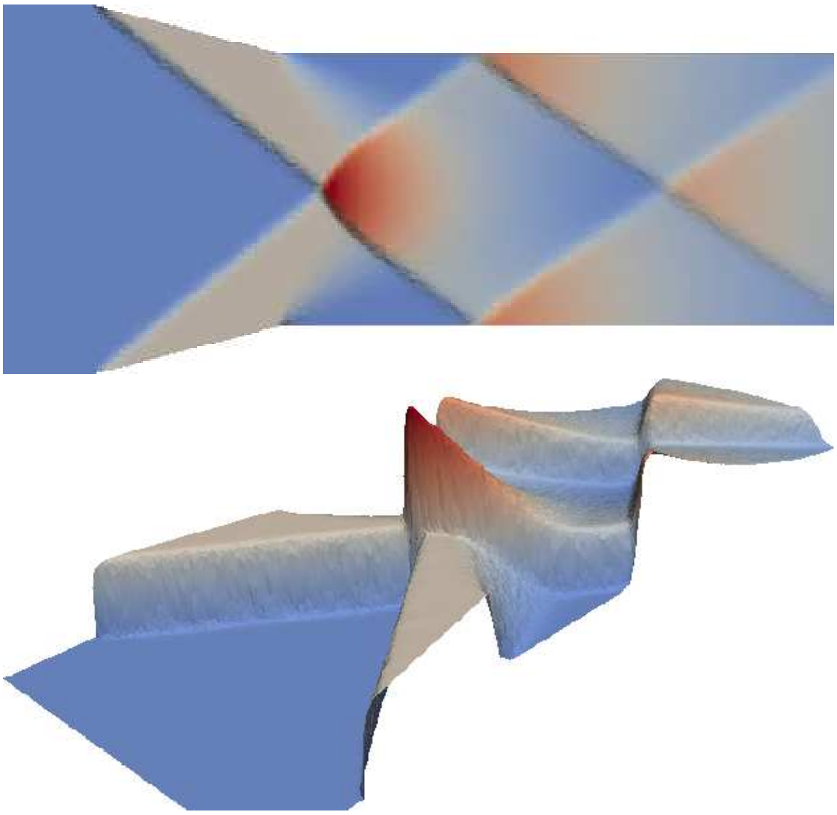

Fig. 19. Water height into a canal with variable geometry for a flat bottom (2D and 3D views).

Next, we consider a non-flat bottom by introducing a bump. The topography is thus defined as follows:

$$z(x,y) = \frac{1}{10} + \frac{3}{2}\left(1 - \frac{(x-30)^2 + (y-20)^2}{5^2}\right)_+ .$$

As presented in figure 20, the bump introduces a large perturbation in the shock wave structure of the solution. In addition, since the bump is larger than the water height, we note a very good behavior of the 2D scheme when approximating wet/dry transitions.

The last performed 2D simulation is devoted to a dam-break perturbed by a large bump. Here, the geometry is a rectangle with $1m$ and $5m$ length. We adopt an unstructured mesh made of 40022 nodes and 79132 triangles. The topography is flat with a bump as follows:

$$z(x,y) = \frac{1}{10} + \frac{3}{2}\left(1 - \frac{(x-5/2)^2 + (y-1/2)^2}{1/25}\right)_+ .$$

We consider a dam-break involving a wet/dry transition. The dam is located at $x = 0.7$ and the initial rest water height is $1.9m$. The obtained simulation is presented in figure 21.

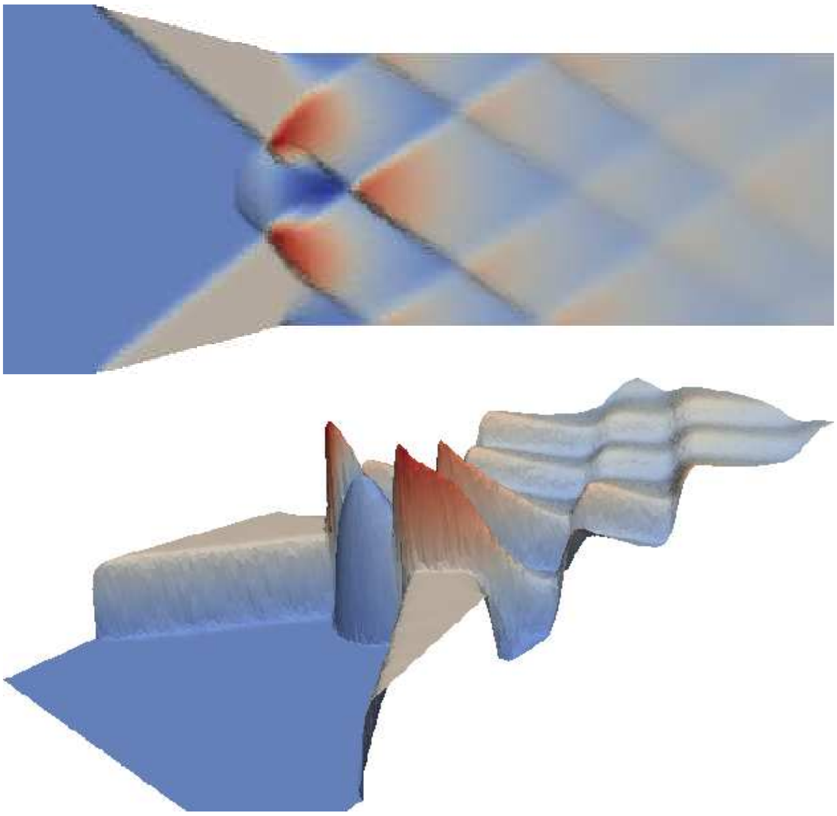

Fig. 20. Water height into a canal with variable geometry for a non flat bottom (2D and 3D views).

7 Conclusion

From a conservative finite volume scheme to approximate the weak solutions of the homogeneous shallow-water equations, we have derived a systematic procedure to deal with non-flat topography. This approach is very easy to be implemented, it is well-balanced and it is non-negative water preserving. It is based on a suitable reformulation of the model where the flux function arguments are nothing else the variables which characterized a steady state at rest.

When compared to the well-known hydrostatic reconstruction, the proposed hydrostatic upwind scheme is able to deal with large variations of the topography on coarse meshes to make this procedure very efficient. In addition, the derivation of second-order accurate extensions is natural and preserves all the expected requirements.

From the 1D scheme, we have proposed a 2D extension on unstructured meshes which preserves all the required robustness properties (well-balance and non-negative bathymetry). In fact, we have shown that the 2D scheme rewrites under an easy formulation which adds to the efficiency of the method. Indeed,

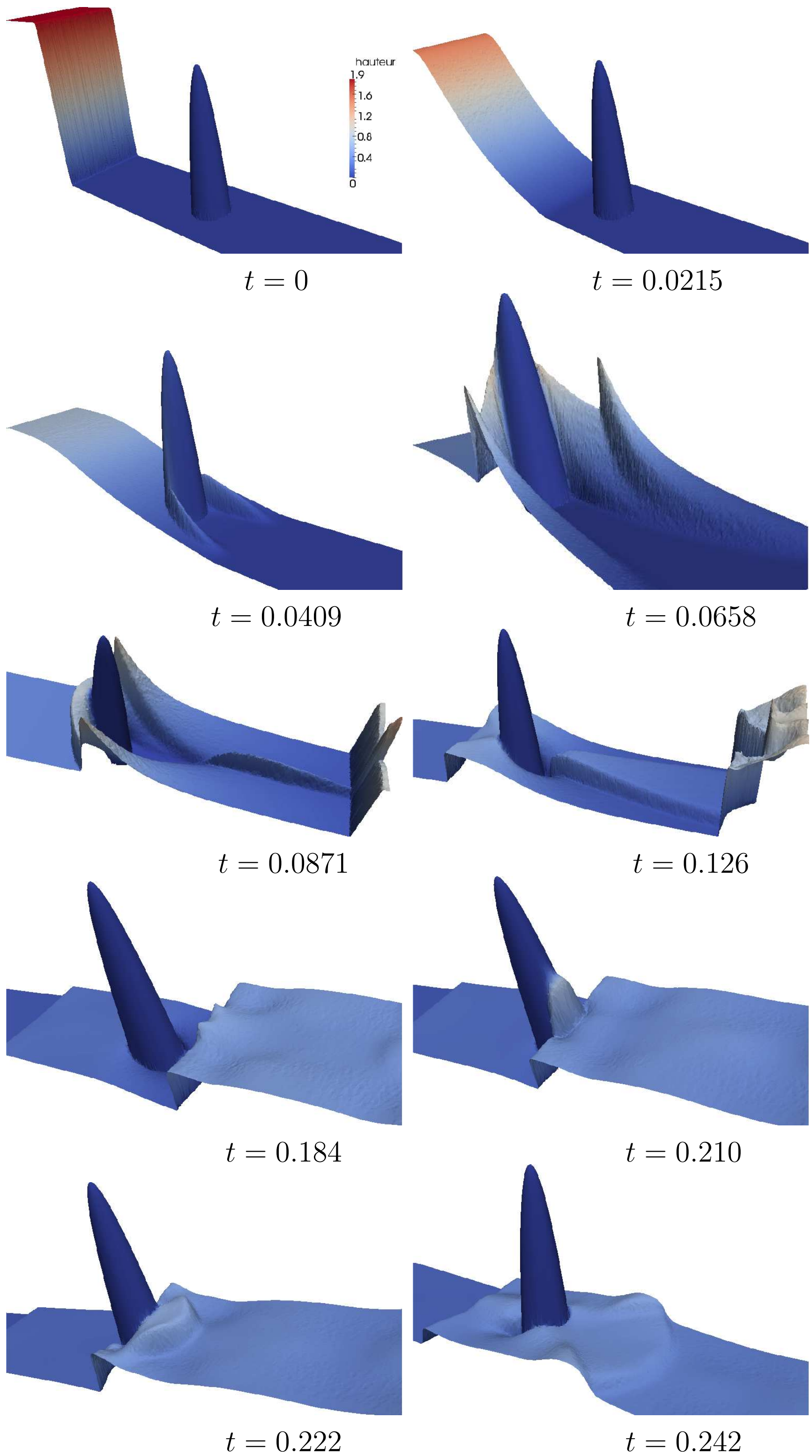

Fig. 21. Water height during a dam-break over a non-flat bottom (3D views).

the suggested hydrostatic upwind scheme can be understood as an obvious correction of any given finite volume scheme on a 2D unstructured mesh, in order to discretize the topography source term.

A lot of numerical experiments have been performed to validate and to illustrate the scheme. Moreover, when considering strong topography variations, the derived hydrostatic upwind scheme produces suitable approximate solutions with the expected behaviors while the well-known hydrostatic reconstruction fails as long as the mesh size is not small enough.

References

[1] E. Audusse, F. Bouchut, M. O. Bristeau, R. Klein, B. Perthame, *A fast and stable well-balanced scheme with hydrostatic reconstruction for shallow water flows*, SIAM J.Sci.Comp., 25, 2050–2065 (2004).

[2] E. Audusse, M.-O. Bristeau, M. Pelanti, J. Sainte-Marie, *Approximation of the hydrostatic Navier-Stokes system for density stratified flows by a multilayer model: kinetic interpretation and numerical solution*, J. Comput. Phys., 230 (2011), 3453-3478.

[3] A. Bermudez, M.E. Vazquez-Cendon, *Upwind Methods for Hyperbolic Conservation Laws with Source Terms*, Computers and Fluids. **23** 1049–1071 (1994).

[4] C. Berthon, *Stability of the MUSCL schemes for the Euler equations*, Comm. Math. Sci., 3, 133–158 (2005).

[5] C. Berthon, *Robustness of MUSCL schemes for 2D unstructured meshes*, J. Comput. Phys., 218, 495–509 (2006).

[6] C. Berthon, *Why the MUSCL-Hancock scheme is* L^1*-stable*, Numer. Math., 104, 27–46 (2006).

[7] C. Berthon, F. Marche, *A positive preserving high order VFRoe scheme for shallow water equations: a class of relaxation schemes*, SIAM J. Sci. Comput. 30 (2008), 2587-2612.

[8] F. Bouchut, *Non-linear stability of finite volume methods for hyperbolic conservation laws and well-balanced schemes for sources*, Frontiers in Mathematics, Birkhauser, 2004.

[9] S. Bryson, Y. Epshteyn, A. Kurganov, G. Petrova, *Well-balanced positivity preserving central-upwind scheme on triangular grids for the Saint-Venant system*, ESAIM Math. Model. Numer. Anal., 45 (2011), 423-446.

[10] T. Buffard, T. Gallouët, J.M. Hérard, *A naive Godunov scheme to solve shallow water equations*, CR Acad. Sci. Paris, 326, 385–390 (1998).

[11] T. Buffard, T. Gallouët, J. M. Hérard, *A sequel to a rough Godunov scheme: application to real gases*, Computers and Fluids, 29, 813–847 (2000).

[12] J. Burguete, P. Garcìa-Navarro, *Efficient construction of high-resolution tvd conservative schemes for esquations with source terms : application to shallow water flows*, International Journal for Numerical Methods in Fluids, 37 (2001), 209-248.

[13] M. Castro, J. Macías, C. Parés, *A Q-scheme for a class of systems of coupled conservation laws with source term. Application to a two-layer 1-D shallow water system*, M2AN Math. Model. Numer. Anal., 35 (2001), pp. 107-127.

[14] M. J. Castro, A. Pardo, C. Parès, *Well-balanced numerical schemes based on a generalized hydrostatic reconstruction technique*, Mathematical Models and Methods in Applied Sciences, 17 (2007), 2065-2113.

[15] E. M. Chaabelasri, N. Salhi, I. Elmahi, F. Benkhaldoun, *High order well balanced scheme for treatment of transcritical flow with topography on adaptive triangular mesh*, Phys. Chem. News, 53 (2010), 119–128.

[16] C. Chalons, J.-J. Coulombel, *Relaxation approximation of the Euler equations*, J. Math. Anal. Appl., 348 (2008), 872-893.

[17] F. Coquel and B. Perthame, *Relaxation of Energy and Approximate Riemann Solvers for General Pressure Laws in Fluid Dynamics*, SIAM J. Numer. Anal., 35, 2223–2249 (1998).

[18] O. Delestre, Simulation du ruisselement d'eau de pluie sur des surfaces agricoles, P.h.D Thesis, University of Orléans (France), 2010.

[19] O. Delestre, C. Lucas, P.-A. Ksinant, F. Darboux, C. Laguerre, T. N. Tuoi Vo, F. James, S. Cordier, *SWASHES: a library of Shallow Water Analytic Solutions for Hydraulic and Environmental Studies*, preprint, HAL hal-00628246 (2011).

[20] T. Gallouët, J. M. Hérard, N.Seguin, *Some approximate Godunov schemes to compute shallow-water equations with topography*, Computers and Fluids, 32, 479–513 (2003).

[21] T. Gallouët, J. M. Hérard, N.Seguin, *On the use of some symetrizing variables to deal with vacuum*, Calcolo, 40, 163–194 (2003).

[22] T.Gallouët, J.M. Hérard, N. Seguin, *Some recent Finite Volume schemes to compute Euler equations using real gas EOS*, Int J. Num. Meth. Fluids, 39, 1073-1138 (2002).

[23] T. Gallouët, T. Masella, *A rough Godunov scheme*, C. R., Math., Acad. Sci. Paris, 323, 77–83 (1996).

[24] J.-F. Gerbeau, B. Perthame, *Derivation of viscous Saint-Venant system for laminar shallow water; numerical validation*, Discrete Contin. Dyn. Syst. Ser. B, 1 (2001) 89102.

[25] E. Godlewski, P.A. Raviart, *Numerical Approximation of Hyperbolic System of Conservation Laws*, Applied Mathematical Sciences, **118**, Springer, New-York, 1996.

[26] L. Gosse, *A well-balanced flux-vector splitting scheme designed for hyperbolic systems of conservation laws with source terms*, Comput. Math. Appl. 39 (2000), 135-159.

[27] N. Goutal, F. Maurel, *A finite volume solver for 1D shallow-water equations applied to an actual river*, Int. J. Numer. Meth. Fluids 38, 119 (2002).

[28] N. Goutal, F. Maurel, *Proceedings of the 2nd workshop on dam-break wave simulation*, Technical report, EDF-DER, HE-43/97/016/B (1997)

[29] J. M. Greenberg, A. Y. Leroux, *A well-balanced scheme for the numerical processing of source terms in hyperbolic equations*, SIAM J. Numer. Anal., 33, 1–16 (1996).

[30] J. M. Greenberg, A. Y. Leroux, R. Baraille, A. Noussair, *Analysis and approximation of conservation laws with source terms*, SIAM J. Numer. Anal., 34, 1980–2007 (1997).

[31] A. Harten, P.D. Lax, B. Van Leer, *On upstream differencing and Godunov-type schemes for hyperbolic conservation laws*, SIAM Review, 25, 35–61 (1983).

[32] S. Jin, *A steady-state capturing method for hyperbolic systems with geometrical source terms*, M2AN Math. Model. Numer. Anal., 35, 631–645 (2001).

[33] S. Jin, X. Wen, *Two interface-type numerical methods for computing hyperbolic systems with geometrical source terms having concentrations*, SIAM J. Sci. Comput., 26, 2079–2101 (2005).

[34] S. Jin, X. Wen, *An efficient method for computing hyperbolic systems with geometrical source terms having concentrations*, Special issue dedicated to the 70th birthday of Professor Zhong-Ci Shi. J. Comput. Math., 22, 230–249 (2004).

[35] S. Jin, Z. Xin, *The Relaxation Scheme for Systems of Conservation Laws in Arbitrary Space Dimension*, Comm. Pure Appl. Math., 45, 235–276 (1995).

[36] F. Lagoutière, *Stability of reconstruction schemes for hyperbolic PDEs*, Communications in Mathematical Sciences, 6 (2008), 57–70.

[37] B. Larrouturou, *How to preserve the mass fractions positivity when computing compressible multi-component flows*, J. Comput. Phys. 95, pp. 59–84 (1991).

[38] B. van Leer, *Towards the ultimate conservative difference scheme. V. A second-order sequel to Godunov's method*, J. Comput. Phys., 32, 101–136 (1979).

[39] G. LeFloch, M.D. Thanh, *The Riemann problem for the shallow water equations with discontinuous topography*, Commun. Math. Sci., 5 (2007), 865-885.

[40] G. LeFloch, M.D. Thanh, *A Godunov-type method for the shallow water equations with discontinuous topography in the resonant regime*, Journal of Computational Physics, 230 (2011), 7631–7660.

[41] R. J. LeVeque, *Finite volume methods for hyperbolic problems*, Cambridge Texts in Applied Mathematics, Cambridge University Press, Cambridge (2002).

[42] R. J. LeVeque, M. Pelanti, *A class of approximate Riemann solvers and their relation to relaxation schemes*, J. Comp. Phys., 172, 572–591 (2001)

[43] F. Marche, *A simple well-balanced model for two-dimensional coastal engineering applications*, Hyperbolic problems: theory, numerics, applications, 271-283, Springer, Berlin, 2008.

[44] T. Morales de Luna, M. J. Castro Díaz, C. Parés, E. Fernández Nieto, *On a shallow water model for the simulation of turbidity currents*, Commun. Comput. Phys. 6 (2009), 848-882.

[45] S. Noelle, N. Pankratz, G. Puppo, J.R. Natvig, *Well-balanced finite volume schemes of arbitrary order of accuracy for shallow water flows*, J. Comp. Phys., 213, 474–499 (2006).

[46] C. Parés, M. Castro, *On the well-balance property of Roe's method for nonconservative hyperbolic systems. Applications to shallow-water systems*, Mathematical Modelling and Numerical Analysis., 38 (2004), 821–852.

[47] B. Perthame, C.W. Shu, *On positivity preserving finite volume schemes for Euler equations*, Numer. Math., 73, 119–130 (1996).

[48] B. Perthame, C. Simeoni, *A kinetic scheme for the Saint-Venant system with a source term*, Calcolo, 38 (2001) 201231.

[49] G. Russo, *Central schemes for conservation laws with application to shallow water equations*, Trends and applications of mathematics to mechanics: STAMM 2002, S. Rionero and G. Romano Eds., Springer-Verlag Italia SRL (2005) 225246.

[50] W. C. Thacker, *Some exact solutions to the nonlinear shallow-water wave equations*, Journal of Fluid Mechanics, 107, 499-508 (1981).

[51] E.F. Toro, Riemann solvers and numerical methods for fluid dynamics, Springer-Verlag,, Thrid Edition, A practical introduction, 2009.

[52] E. F. Toro, M. Spruce, W. Speare, *Restoration of the contact surface in the HLL Riemann solver*, Shock waves, 4, 25–34 (2994).

[53] Y. Xing, C.W. Shu, *High order finite difference WENO schemes with the exact conservation property for the shallow water equations*, J. Comp. Phys., 208, 206–227 (2005).